Three-dimensional nematic spin liquid in a stacked triangular lattice 6H-B structure

Kyusung Hwang, Tyler Dodds, Subhro Bhattacharjee, and Yong Baek Kim

Phys. Rev. B **87**, 235103 — Published 3 June 2013

DOI: 10.1103/PhysRevB.87.235103

Three-dimensional nematic spin liquid in the stacked triangular lattice 6H-B structure

Kyusung Hwang,[1] Tyler Dodds,[1] Subhro Bhattacharjee,[1,2] and Yong Baek Kim[1,3]

[1] *Department of Physics and Centre for Quantum Materials, University of Toronto, Toronto, Ontario M5S 1A7, Canada*

[2] *Department of Physics and Astronomy, McMaster University, Hamilton, Ontario L8S 4M1, Canada*

[3] *School of Physics, Korea Institute for Advanced Study, Seoul 130-722, Korea*

(Dated: May 6, 2013)

Recently, a number of experiments indicate the possible presence of spin liquid phases in quantum magnets with spin-1/2 and spin-1 moments sitting on triangular-lattice-based structures in $Ba_3CuSb_2O_9$ and $Ba_3NiSb_2O_9$ respectively. In relation to these experiments, several theoretical proposals have been made for spin liquid phases and spin-liquid-like behaviours on the stacked triangular lattice. While the crystal structures of these materials are currently under debate, it is nonetheless interesting to understand possible spin liquid phases on such frustrated lattices. In this work, we apply Schwinger boson mean-field theory and projective symmetry group (PSG) analysis to investigate spin liquid phases on the fully three-dimensional 6H-B structure, in contrast to previous works that considered two-dimensional systems. We find that a nematic Z_2 spin liquid phase, where the lattice-rotational symmetry is spontaneously broken, is the most promising spin liquid phase that is consistent with spiral magnetic ordering in the classical limit. We discuss the implications of our results to future theoretical and experimental works.

PACS numbers: 75.10.Jm, 75.10.Kt

I. INTRODUCTION

Spin-1/2 moments on two or three dimensional lattices may not order, even at zero temperature, owing to competing interactions and/or quantum fluctuations and form a highly entangled state of quantum matter.[1–8] Such a correlated state, called a quantum spin liquid (QSL),[1–5] is capable of supporting quasiparticle excitations that carry only a fraction of the quantum numbers of the underlying electrons that make up the spin system.

This possibility of emergent quantum number fractionalization and other exotic excitations like *artificial* photons,[2] resulting from strong many-body correlation effects in condensed matter systems, have fuelled massive interest in quantum spin liquids both theoretically and experimentally. A large number of Mott insulators in various frustrated lattice geometries have been investigated, and several candidate materials have been identified.[4,5] Most of these materials, such as κ-(BEDT-TTF)$_2$Cu$_2$(CN)$_3$,[9] Cs_2CuCl_4,[10] EtMe$_3$Sb[Pd(dmit)$_2$]$_2$,[11] (spin-1/2 on triangular lattice) and Herbertsmithite ($ZnCu_3(OH)_6Cl_2$, spin-1/2 kagome lattice)[12–14] are two dimensional. However, some three dimensional systems, like the hyper-kagome lattice $Na_4Ir_3O_8$,[15] several candidate quantum spin-ice materials on the pyrochlore lattices,[16] and more recently the stacked compounds $Ba_3CuSb_2O_9$[17–19] (S=1/2) and $Ba_3NiSb_2O_9$[20] (S=1) have shown much promise. In the light of the above developments, it is useful to explore and understand the behaviour of quantum spin liquids in associated frustrated three dimensional lattices.

In this paper, we study bosonic spin liquids that can be realized in quantum magnets on a three dimensional crystal structure built by stacking triangular lattices in a staggered fashion. This so-called 6H-B phase is obtained in the P6$_3$/*mmc* lattice structure, as shown in Fig. 1. In particular, we focus on a spin-1/2 antiferromagnetic Heisenberg model with intra-layer and inter-layer spin exchanges. The two interactions compete and the model is frustrated when the intra and inter-layer exchanges are comparable. While earlier studies on the 2D honeycomb limit found interesting ground state degeneracies and non-collinear magnetic states selected by quantum order-by disorder,[28] our Schwinger boson mean field theory (SBMFT) captures a *3D Z_2 spin liquid*, a *3D $U(1)$ spin liquid* and a layered, effectively *2D, Z_2 spin liquid* in addition to the usual magnetically ordered phases. Using projective symmetry group (PSG) classification for the

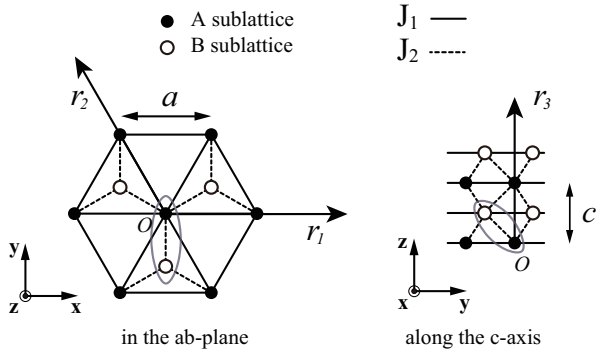

FIG. 1. The 6H-B lattice structure and coordinate system used throughout the paper. The 6H-B lattice consists of the AB-stacked triangular lattices in three dimensions. The left figure shows neighboring two sublattices projected into the *ab*-plane. For the B sublattice, the couplings with J_1 are omitted to simplify the figure. The right figure shows the lattice structure along the *c*-axis. The ellipse indicates the unit cell located at the origin of the coordinate system. $\mathbf{r}_1, \mathbf{r}_2, \mathbf{r}_3$ denotes the three axes of lattice translation.

spin-liquids,[2,38] we find the above bosonic spin liquids that are consistent with various lattice symmetries. A central finding of our SBMFT study is that a 3D *nematic* Z_2 spin liquid, which spontaneously breaks lattice rotation symmetries, is found to be energetically more stable than an isotropic Z_2 spin liquid in the corresponding parameter regime. Interestingly, we find that, unlike the isotropic case, the nematic spin liquid is naturally connected to the classical magnetic orders. The breaking of lattice rotation symmetry in the nematic spin liquid bears a characteristic signature in the two-spinon excitation spectrum for the nematic spin liquid. Such two-spinon spectrum is relevant to neutron scattering experiments. Within mean-field theory we find several quantum phase transitions among spin-liquids, and between spin-liquids and magnetically ordered phases. While some of them, like the transition between the collinear Néel and the 3D $U(1)$ spin liquid, are most likely rendered discontinuous by gauge fluctuations beyond the mean field, others like the transition between the 3D, Z_2 and the spiral are likely to remain continuous. The transition between various magnetically ordered phases and the spin liquids can be understood in terms of condensation of the spinons[29,30] and a charge-2 Higgs field (discussed later).

As noted earlier, a partial motivation for studying the above spin model in this lattice structure stems from recent interests in two new candidate QSLs, viz., $Ba_3CuSb_2O_9$ (spin-1/2) and (6H-B-)$Ba_3NiSb_2O_9$, (spin-1) where initial experiments suggested a 6H-B structure.[17,18,20] These compounds do not show magnetic order down to a few hundred mK, despite Curie-Weiss temperatures, as measured from the high temperature susceptibility, (greater than 50 K). Furthermore, they show a large intermediate temperature window where the magnetic specific heat shows a linear temperature dependence suggesting the possibility of an unconventional spin state. While recent experiments on the spin-1/2 Cu compound revealed a different crystal structure for $Ba_3CuSb_2O_9$,[17,18,27] it may be still useful to think about possible spin-1/2 and/or spin-1 spin liquids on the 6H-B phase in search of three dimensional spin liquids and possible exotic quantum phase transitions. This approach is in contrast to the previous theoretical studies that mainly considered two dimensional spin models for the compounds.[21–27]

The rest of this paper is structured as follows. In Sec. II, we give an overview of the $P6_3/mmc$ lattice structure obtained in the 6H-B phase, discuss its symmetries, and introduce a frustrated Heisenberg model. Next, we discuss the Schwinger boson formalism in Sec. III, and derive the mean-field Hamiltonian, which can describe the transition between classical order and as well as a regime of stronger quantum fluctuations. To classify distinct mean-field ansätze with a given symmetry, we introduce the PSG analysis in Sec. IV, and describe the allowed ansatz with the full symmetry of the lattice, along with those that break lattice rotational symmetry spontaneously. We work out the magnetic phases obtained in the classical limit of our model in Sec. V, and note that this behaviour cannot be fully captured from the symmetric spin liquid ansatz. In fact, we find that the symmetric spin liquid is generally energetically inferior to the nematic spin liquid in the relevant part of the SBMFT phase diagram. The full phase diagrams as a function of κ and J_2/J_1 for the different ansätze are discussed in Sec. VI. We also point out the nature of different phase transitions and indicate the underlying mechanisms to study them. Finally, the structure of the two-spinon excitations is discussed in Sec. VII. We end by summarizing our results and discussing their implications in Sec. VIII. The details of the PSG calculations, derivations of the ansätze and other details are given in different appendices.

II. LATTICE STRUCTURE AND SPIN HAMILTONIAN FOR THE 6H-B PHASE

The 6H-B structure may be thought of as a collection of triangular lattices stacked along the c-axis, with two consecutive layers being offset as shown in Fig. 1. Sites on even layers form the triangular A sublattice. Those on odd layers form the triangular B sublattice, and are offset above the centre of the triangles of the A sublattice.

On such a lattice, we consider a spin-1/2 model where the predominant interactions between spins on the lattice are nearest-neighbour antiferromagnetic super-exchange interactions. Interactions within the A and B triangular planes have strength J_1, and those between neighbouring planes have strength J_2. Both couplings may be comparable in the case of systems such as $Ba_3CuSb_2O_9$, where the exchange paths are mediated through intermediate oxygen atoms. The resulting Heisenberg Hamiltonian is

$$H = J_1 \sum_{\langle i,j\rangle \text{ in plane}} \mathbf{S}_i \cdot \mathbf{S}_j + J_2 \sum_{\langle i,j\rangle \text{ between planes}} \mathbf{S}_i \cdot \mathbf{S}_j, \qquad (1)$$

where $J_1,\ J_2 > 0$.

This model has two simple limits: (i) $J_1 \gg J_2$ and (ii) $J_1 \ll J_2$. In the first case, the model is reduced to the two-dimensional triangular lattice Heisenberg model. It is well known that the ground state of the model has 120° non-collinear (spiral) Néel order.[31] In the other limit, the system has a three-dimensional bipartite lattice structure without frustration so that it allows collinear Néel order as its ground state.[32] However, in the regime where both couplings are comparable ($J_1 \approx J_2$), the interactions compete with each other, and this may lead to a quantum spin liquid ground state. At this point, we also note (as discussed in detail later) that in the classical limit, the above spin model has the spiral ordered ground state in the intermediate region of coupling constants (see Fig. 4).

We proceed by noting various symmetries of the spin model in anticipation of our future Projective Symmetry Group calculation. The lattice is described by the

following primitive vectors, as seen in Fig. 1:

$$\mathbf{R}_1 = a\hat{x}, \mathbf{R}_2 = a\left(-\frac{1}{2}\hat{x} + \frac{\sqrt{3}}{2}\hat{y}\right), \mathbf{R}_3 = c\hat{z}, \quad (2)$$

where a and c are the sublattice spacings in the a-b plane and along the c-axis, respectively. We write lattice coordinates as $\mathbf{r}_A = \sum_{n=1}^{3} r_n \mathbf{R}_n \equiv (r_1, r_2, r_3)_A$ for the A sublattice, and $\mathbf{r}_B = \mathbf{r}_A + \mathbf{r}_{BA} \equiv (r_1, r_2, r_3)_B$ for the B sublattice, where $\mathbf{r}_{BA} = -\mathbf{R}_1/3 - 2\mathbf{R}_2/3 + \mathbf{R}_3/2$. In this coordinate representation, r_n $(n = 1, 2, 3)$ is an integer. The system has the following symmetries: spin-rotation, time-reversal, and space group symmetries. The first two symmetries are discussed in the next sections. The spin model (1) has the space group $P6_3/mmc$ with following seven generators:[33]

- Translations T_1 and T_2 within the triangular plane, and another, T_3, along the c-axis.
- A 120°-rotation R around the z-axis, centered on an A site.
- A reflection Π_1 through the y-z plane, and another, Π_2, through the x-y plane.
- An inversion Ξ through the midpoint between neighbouring A and B sites.

Consequently, the space group transformations are defined as

$$T_1 : (r_1, r_2, r_3)_p \to (r_1 + 1, r_2, r_3)_p, \quad (3a)$$
$$T_2 : (r_1, r_2, r_3)_p \to (r_1, r_2 + 1, r_3)_p, \quad (3b)$$
$$T_3 : (r_1, r_2, r_3)_p \to (r_1, r_2, r_3 + 1)_p, \quad (3c)$$
$$R : (r_1, r_2, r_3)_p \to (-r_2 + \delta_{p,B}, r_1 - r_2 + \delta_{p,B}, r_3)_{\bar{p}}, \quad (3d)$$
$$\Pi_1 : (r_1, r_2, r_3)_p \to (-r_1 + r_2, r_2, r_3)_{\bar{p}}, \quad (3e)$$
$$\Pi_2 : (r_1, r_2, r_3)_p \to (r_1, r_2, -r_3 - \delta_{p,B})_{\bar{p}}, \quad (3f)$$
$$\Xi : (r_1, r_2, r_3)_p \to (-r_1, -r_2, -r_3)_{\bar{p}}, \quad (3g)$$

where p $(\bar{p}) = A, B$ (B, A) refers to the two sublattices.

Having determined the symmetries of our spin model, in the next section we begin our Schwinger boson mean-field analysis, and proceed to identify the various possible bosonic spin liquids within a projective representation of the above symmetry group.

III. SCHWINGER BOSON MEAN-FIELD THEORY AND GAUGE STRUCTURE

In the Schwinger boson mean-field theory,[34–36] the spin operator at site i is represented in terms of bosonic spinons $b_{i\mu}$:

$$S_i^a = \frac{1}{2} b_{i\mu}^\dagger \sigma_{\mu\nu}^a b_{i\nu}, \quad (4)$$

where $a = x, y, z$, $\mu, \nu = \uparrow, \downarrow$, $\{\sigma^a\}$ are the Pauli matrices, and a sum over repeated Greek indices is assumed hereafter. In this formalism, operators of any spin quantum number S can be represented, which is given by the on-site density constraint,

$$\kappa = b_{i\mu}^\dagger b_{i\mu} = 2S. \quad (5)$$

Within the mean-field theory, the constraint is implemented on average. In general, $\kappa/2$ represents the spin quantum number and acts as a parameter that determines the degree to which quantum fluctuations are important to our Hamiltonian. The κ $(\sim S) \to \infty$ limit corresponds to classical limit.[36]

Following the usual SBMFT techniques,[35,36] we now consider the mean-field decoupling of the Heisenberg terms. With the help of the constraint (5), we can rewrite these terms as

$$\mathbf{S}_i \cdot \mathbf{S}_j = -\frac{1}{2}\hat{\eta}_{ij}^\dagger \hat{\eta}_{ij} + \frac{\kappa^2}{4}, \quad (6)$$

where $\hat{\eta}_{ij} = b_{i\mu}\epsilon_{\mu\nu}b_{j\nu}$ and $\epsilon_{\mu\nu}$ is totally antisymmetric tensor with $\epsilon_{\uparrow\downarrow} = 1$. In this form, the mean-field decoupling is straightforward. After the mean-field decoupling, we employ a Lagrange multiplier, λ_i, for each site to implement the constraint (5). In the resulting quadratic mean-field Hamiltonian, we introduce the parameter $x_{i\mu} = \langle b_{i\mu} \rangle$ which represents the bosonic condensate fraction:

$$b_{i\mu} \to x_{i\mu} + b_{i\mu}. \quad (7)$$

Now $b_{i\mu}$ implies the noncondensate part of the original bosonic spinon. If $x_{i\mu} \neq 0$, there is condensation of the spinons, and hence a long range magnetically ordered state with spontaneously broken spin-rotation symmetry. However, if the spinons are gapped then there is no condensate, and the spin-rotation symmetry is preserved. This is a spin liquid state with gapped bosonic spin-1/2 (spinon) excitations. In three dimensions, it can be either a Z_2 or U(1) spin liquid. In the former case, in addition to the spinons, there is an emergent gapped non-magnetic excitation called the *vison*.[37] On the other hand, in the U(1) spin liquid, there is an emergent gapless *photon* (with two polarization modes) and a gapped magnetic monopole excitation.[2] These issues are discussed in some detail later. The mean-field Hamiltonian is written as

$$\begin{aligned} H_{MF} = &\sum_{i>j}\left(-\frac{1}{2}J_{ij}\eta_{ij}\right) b_{i\mu}^\dagger \epsilon_{\mu\nu} b_{j\nu}^\dagger + \text{H.c.} \\ &+ \sum_{i>j}\left(-\frac{1}{2}J_{ij}\eta_{ij}\right)\left(x_{i\mu}^* \epsilon_{\mu\nu} x_{j\nu}^*\right) + \text{c.c.}, \\ &+ \sum_i \lambda_i \left(b_{i\mu}^\dagger b_{i\mu} + |x_{i\mu}|^2 - \kappa\right) \\ &+ \sum_{i>j}\left(\frac{1}{2}J_{ij}\left|\eta_{ij}\right|^2 + \frac{1}{4}J_{ij}\kappa^2\right) \end{aligned} \quad (8)$$

where $\eta_{ij} = x_{i\mu}\epsilon_{\mu\nu}x_{j\nu} + \langle b_{i\mu}\epsilon_{\mu\nu}b_{j\nu}\rangle$ is the mean-field expectation value of the bond parameter. The above mean-field Hamiltonian is then solved self-consistently using the following saddle-point equations:

$$\frac{\partial\langle H_{MF}\rangle}{\partial\eta^*_{ij}} = 0, \quad \frac{\partial\langle H_{MF}\rangle}{\partial x^*_{i\mu}} = 0, \quad \frac{\partial\langle H_{MF}\rangle}{\partial\lambda_i} = 0. \tag{9}$$

There exists a $U(1)$ gauge redundancy in the Schwinger boson representation of the spin operator (4). That is, under the transformation

$$b_{i\mu} \to e^{i\phi_i}b_{i\mu}, \tag{10}$$

the spin operator $\mathbf{S}_i$ in (4) is invariant. However, the mean-field parameter transforms as

$$\eta_{ij} \to e^{-i(\phi_i+\phi_j)}\eta_{ij}. \tag{11}$$

For non-bipartite lattices, when a particular mean-field state is chosen such that $\eta_{ij} \neq 0$ is fixed, the above $U(1)$ gauge invariance is broken down to Z_2, since now the mean-field Hamiltonian is gauge invariant only for $\phi_i = 0, \pi$.[2,38] The resulting state is a Z_2 spin liquid. The gauge redundancy described above, however, suggests that different Z_2 spin liquid ansätze may be connected by gauge transformations and hence correspond to the same physical state.

In the next section, we provide the classification scheme for physically distinct Z_2 spin liquid phases, using a PSG analysis.[2,38]

IV. PROJECTIVE SYMMETRY GROUP ANALYSIS FOR THE MEAN-FIELD ANSÄTZE

A. Brief Overview

At the mean-field level, different spin liquids are characterized by different PSGs, which are projective extensions of the symmetry group of the Hamiltonian.[2,38,47]

For a given spin liquid ansatz (in our case a choice of η_{ij}), the PSG is the set of operations $\{G_X X\}$, where X is an element of the symmetry group and G_X is the associated gauge transformation, that leave the mean-field Hamiltonian invariant. Here, we will describe the general framework to determine $\{G_X\}$ for a particular symmetry group (SG). The details of the calculations are given in Appendix A and B. Note that this analysis characterizes spin-liquid states without long-range order; that is, mean-field Hamiltonians (8) in the absence of a condensate $x_{i\mu}$. Considering the case of Z_2 spin liquids, we define

$$h_{ij} \equiv \eta_{ij}b^\dagger_{i\mu}\epsilon_{\mu\nu}b^\dagger_{j\nu}, \tag{12}$$

and find that under the combined effect of a symmetry transformation, X, and associated gauge transformation G_X, we have

$$(G_X X)h_{ij} = \eta_{ij}e^{-i(\phi_X[X(i)]+\phi_X[X(j)])}b^\dagger_{X(i)\mu}\epsilon_{\mu\nu}b^\dagger_{X(j)\nu}. \tag{13}$$

Hence, for $\{G_X X\}$ that leave H_{MF} invariant, symmetry-related mean-field parameters are found by

$$\eta_{X(i)X(j)} = \eta_{ij}e^{-i(\phi_X[X(i)]+\phi_X[X(j)])}. \tag{14}$$

As mentioned in Sec. III, gauge transformations generally change H_{MF}, but a particular subset, called the Invariant Gauge Group (IGG) of the PSG, may leave it invariant. The IGG is a projective extension of the identity operation of the symmetry group. One can choose a gauge in which the IGG is independent of the site.[2] For Z_2 spin liquids, IGG=$\{+1, -1\}$. The structure of the IGG determines the nature of the low-energy gauge fluctuations around H_{MF}. For Z_2 spin liquids, these fluctuations are gapped. There is a gapped non-magnetic vortex-like excitation that carries the flux of the Z_2 gauge field. However, for $U(1)$ spin liquids, there is an emergent gapless photon, as well as a gapped magnetic monopole excitation, the latter resulting from the compactness of the U(1) gauge group.[2]

We note that if $G_X X$ leaves H_{MF} invariant, so does $WG_X X$ for $W \in$ IGG, which means that a class of G_X is defined only up to elements of the IGG. To generate restrictions for $\{G_X\}$, we note that products of $G_{X_a}X_a$ that are physically equivalent to an identity transformation must be in the IGG.[2,38] Since each operation leaves H_{MF} invariant, the total transformation has no net physical transformation and also leaves H_{MF} invariant. Multiplication rules among the generators of the symmetry group generate precisely these products of transformations. We write these rules in the form $X_a X_b X_c^{-1} X_d^{-1} = I$, and note that upon inclusion of the corresponding gauge transformations, we have

$$(G_{X_a}X_a)(G_{X_b}X_b)(G_{X_c}X_c)^{-1}(G_{X_d}X_d)^{-1} \in \text{IGG}. \tag{15}$$

Motivated by the classical solution of the Heisenberg model (1) (as determined in Sec. IV), we consider two sets of symmetry groups.

$$\text{SG}_1 = \text{Span}\{T_1, T_2, T_3, \Pi_1, \Pi_2, \Xi\}, \tag{16a}$$
$$\text{SG}_2 = \text{Span}\{T_1, T_2, T_3, \Pi_1, \Pi_2, \Xi, R\}. \tag{16b}$$

The group SG_2 consists of the full set of lattice symmetries given in (3). However, we will find that the resulting ansatz with SG_2 is too restrictive to be consistent with the classical limit of this model. We find that it does not lead to the right magnetic ordered state in the classical limit. Thus, we also consider the symmetry group $\text{SG}_1 (\subset \text{SG}_2)$ by removing the rotation R, which will be shown to provide a spin liquid phase consistent with the spiral magnetic order in the classical limit. For each of these symmetry groups, we find the gauge transformations $\{G_X\}$ associated with the symmetry operations, and generate the resulting ansätze H_{MF} using Eq. (14).

B. Z_2 Spin Liquid Ansätze

In this subsection, we discuss the ansätze for both symmetry groups SG_1 and SG_2. A brief sketch of their

derivation is given in Appendix C. Mean-field Hamiltonians for the ansätze are provided in Appendix D.

We find four different ansätze for SG_1 and only one ansatz for SG_2. The ansätze are differentiated by the gauge fluxes of $\{\eta_{ij}\}$ through various loops with even length. The gauge flux Φ on a loop with length $2n$ is defined through

$$\begin{aligned}&\eta_{i_1 i_2}(-\eta^*_{i_2 i_3})\cdots\eta_{i_{2n-1}i_{2n}}(-\eta^*_{i_{2n}i_1})\\&=|\eta_{i_1 i_2}||\eta_{i_2 i_3}|\cdots|\eta_{i_{2n-1}i_{2n}}||\eta_{i_{2n}i_1}|\cdot e^{i\Phi}.\end{aligned}\tag{17}$$

Under the effects of a gauge transformation, (11), this flux is invariant, providing a clear way to distinguish among the ansätze that have the same symmetry group.[39] To differentiate the ansätze, we consider the gauge fluxes on the three kinds of loops shown in Fig. 2. Filled and empty circles denote neighboring A and B sublattices, viewed along c-axis. The flux Φ_1 is defined in any rhombus on each triangular sublattice layer., Φ_1' is the flux defined in any hexagonal loop between neighboring sublattice layers. The last flux is Φ_2 on a kite-shaped loop. For the ansätze of SG_1, the loop consists four different mean-field links $\{\eta_{1\alpha},\eta_{1\beta},\eta_{2\alpha},\eta_{2\beta}\}$, which will be defined below. The three fluxes for the ansätze of SG_1 are listed in Table I. Interestingly, $\Phi_1=\Phi_1'$ for the four ansätze of SG_1. The ansätze are named with the gauge-invariant fluxes (Φ_1,Φ_2).

a. SG_1: As mentioned above, four different ansätze are found for the symmetry group SG_1: the $(0,0)$-flux ansatz, $(0,\pi)$-flux ansatz, $(\pi,0)$-flux ansatz, and (π,π)-flux ansatz.

The $(0,0)$-flux ansatz and $(0,\pi)$-flux ansatz are depicted in Fig. 3. Both ansätze are translationally invariant. To explicitly preserve time-reversal symmetry, we work in a gauge where these ansätze have real-valued mean-field parameters η_{ij}. Since $\eta_{ji}=-\eta_{ij}$, we denote the directions of the positive parameters in Fig. 3. In the symmetry group SG_1, due to the lack of rotational symmetry, there are two different in-plane mean-field parameter magnitudes $\eta_{1\alpha}$ and $\eta_{1\beta}$, and two inter-plane ones $\eta_{2\alpha}$ and $\eta_{2\beta}$.

TABLE I. Classification of the mean-field ansätze of SG_1. Φ_1, Φ_1', Φ_2 are defined on the closed loops in Fig. 2. n_1 (= 0 or 1) is an integer variable characterizing the projective symmetry group of SG_1 [see (A16)]. m (= 0 or 1) is an integer variable reflecting the phase difference among the four mean-field parameters, $\eta_{1\alpha}$, $\eta_{1\beta}$, $\eta_{2\alpha}$, $\eta_{2\beta}$ [defined in (C4)]. n_s is the number of sites in a unit cell. $\mathbf{R}_2'=\mathbf{R}_1+2\mathbf{R}_2$. The $(0,0)$-flux and $(0,\pi)$-flux ansätze are translationally invariant, whereas the $(\pi,0)$-flux and (π,π)-flux ansätze are not invariant. The latter ansätze have doubled unit cell with four sites. The $(0,\pi)$-flux ansatz for SG_1 includes the ansatz for SG_2 as a special case with $\eta_{1\alpha}=\eta_{1\beta}$ and $\eta_{2\alpha}=\eta_{2\beta}$.

ansatz	$\Phi_1=\Phi_1'$	Φ_2	n_1	m	n_s	lattice vectors
$(0,0)$-flux	0	0	0	1	2	$\{\mathbf{R}_1,\mathbf{R}_2,\mathbf{R}_3\}$
$(0,\pi)$-flux	0	π	0	0	2	$\{\mathbf{R}_1,\mathbf{R}_2,\mathbf{R}_3\}$
$(\pi,0)$-flux	π	0	1	0	4	$\{\mathbf{R}_1,\mathbf{R}_2',\mathbf{R}_3\}$
(π,π)-flux	π	π	1	1	4	$\{\mathbf{R}_1,\mathbf{R}_2',\mathbf{R}_3\}$

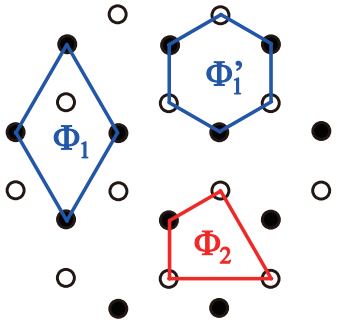

FIG. 2. Gauge fluxes to differentiate the ansätze of SG_1 and the loops where they are defined. The gauge flux on each loop is defined with (17). The values of the fluxes for the ansätze are listed in Table I.

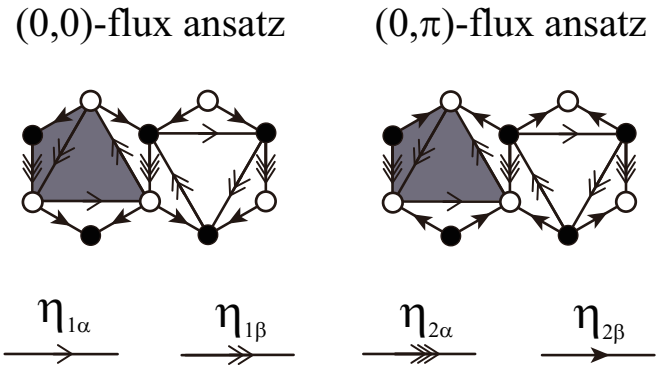

FIG. 3. $(0,0)$-flux ansatz and $(0,\pi)$-flux ansatz of the symmetry group SG_1. The figure shows the directions and magnitudes of the allowed mean-field parameters, viewed along the c-axis. Filled and empty circles denote A and B sublattices, respectively. Arrows indicate the directions of the four allowed positive, real mean-field parameters $\eta_{1\alpha}$, $\eta_{1\beta}$, $\eta_{2\alpha}$, and $\eta_{2\beta}$. The shaded region indicates the inside of the three-dimensional path around which the gauge flux Φ_2 is defined. The flux Φ_2 distinguishes the two ansätze.

The (0,0)- and (0,π)-flux ansätze are distinguished by the flux Φ_2. The shaded region in Fig. 3 indicates the inside of the loop where Φ_2 is defined. In fact, the flux Φ_2 is defined only when every η_{ij} along the loop is non-zero. In the mean-field theory, we will come across two special cases with $\eta_{1\alpha}=\eta_{1\beta}\equiv\eta_1$ and $\eta_{2\alpha}=\eta_{2\beta}\equiv\eta_2$: one where $\eta_1=0$, and the other where $\eta_2=0$. In the first case, $\eta_1=0$, our (0,0)- and (0,π)-flux ansätze become gauge-equivalent. Furthermore, the connectivity changes so that the two sublattices become bipartite. As we show later, in this case we actually have a three-dimensional gapped $U(1)$ spin liquid, which is in principle a stable phase, unlike in two dimensions. We denote this as the 3D-$U(1)$ state. In the second case, $\eta_2=0$, our two ansätze are identical, giving a two-dimensional Z_2 spin liquid with zero flux through rhombus plaquettes in the triangular planes ($\Phi_1=0$). We denote this as the 2D-Z_2

state. It is one of the two Z_2 spin liquids allowed with the symmetry of the 2D triangular lattice.[38] The symmetry group of the 6H-B structure does not include the 2D triangular lattice symmetry group as a subgroup, due to the lack of the six-fold rotational symmetry. As a result, the PSG analysis on the 6H-B structure, in the 2D limit, recovers only the Z_2 spin liquid with zero flux within the rhombus plaquettes in the triangular planes. The other Z_2 spin liquid with π flux of the 2D triangular lattice appears as a saddle point, not the energy minimum, in the $J_2 = 0$ limit of (π,0)- and (π,π)-flux ansätze. For details, readers are referred to Appendix E.

Before moving on to the case of SG_2, we briefly mention about the $(\pi, 0)$-flux and (π,π)-flux ansätze. Those ansätze are not manifestly invariant under translation. They break the translation symmetry along r_2-direction so that they have doubled unit cell with four sites. The mean-field configurations of the ansätze are shown in Fig. 13.

b. SG_2: The PSG analysis of the full symmetry group SG_2 finds only one allowed ansatz, which has $\Phi_1 = \Phi_1' = 0$ and $\Phi_2 = \pi$. This is related to the (0,π)-flux ansatz with SG_1, for the case where the mean-field magnitudes acquire rotational symmetry, *i.e.*, $\eta_{1\alpha} = \eta_{1\beta}$ and $\eta_{2\alpha} = \eta_{2\beta}$. Thus, the (0,$\pi$)-flux ansatz for SG_1 includes the ansatz for SG_2 as a special case.

Having discussed the allowed ansätze for our symmetry groups SG_1 and SG_2, we consider the phases obtained in different parameter regimes.

V. CLASSICAL ORDERING

We begin by studying the classical ground state of the spin model (1), in the context of Schwinger boson mean-field theory. The classical limit is obtained by taking the $\kappa \to \infty$ limit of the SBMFT. From the scaling behavior of the mean-field solution for $\kappa \gg 1$, ($\eta_{ij} \sim \kappa$, $x_{i\mu} \sim \sqrt{\kappa}$, $\lambda \sim \kappa$) the ground state energy can be written as[36]

$$E_c = \frac{\langle H_{MF}\rangle}{\kappa^2} = \sum_{i>j}\left(\frac{J_{ij}}{2}|\tilde{\eta}_{ij}|^2 + \frac{J_{ij}}{4}\right) + \sum_{i>j}\left(-\frac{J_{ij}}{2}\tilde{\eta}_{ij}\right)\left(\tilde{x}^*_{i\mu}\epsilon_{\mu\nu}\tilde{x}^*_{j\nu}\right) + \text{c.c.} + \sum_i \tilde{\lambda}_i\left(|\tilde{x}_{i\mu}|^2 - 1\right), \tag{18}$$

In the above expressions, $\tilde{\eta}_{ij} = \eta_{ij}/\kappa$, $\tilde{x}_{i\mu} = x_{i\mu}/\sqrt{\kappa}$, $\tilde{\lambda} = \lambda/\kappa$. The ground state is determined by solving the following mean-field equations:

$$\frac{\partial E_c}{\partial \tilde{\eta}^*_{ij}} = 0, \quad \frac{\partial E_c}{\partial \tilde{x}^*_{i\mu}} = 0, \quad \frac{\partial E_c}{\partial \tilde{\lambda}_i} = 0. \tag{19}$$

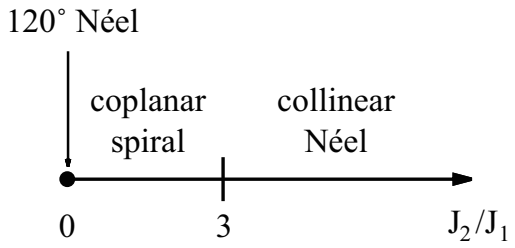

FIG. 4. Phase diagram of classical magnetic order of the Hamiltonian (1) as a function of J_2/J_1.

Making use of the above mean-field equations, we rewrite the ground state energy as

$$E_c = \sum_{i>j}\frac{J_{ij}}{4}\mathbf{S}^c_i \cdot \mathbf{S}^c_j + \sum_i \tilde{\lambda}_i\left(|\mathbf{S}^c_i| - 1\right), \tag{20}$$

where the classical spin vector is given by

$$\mathbf{S}^c_i = \tilde{x}^*_{i\mu}\boldsymbol{\sigma}_{\mu\nu}\tilde{x}_{i\nu}. \tag{21}$$

This is precisely the classical Heisenberg model with the constraint of normalized spin vectors. The solution of (20) can be obtained via the Luttinger-Tisza method[48–50] as follows:

$$\mathbf{S}^c_A(\mathbf{r}) = \mathbf{n}_1\cos[\mathbf{Q}_c\cdot\mathbf{r}] + \mathbf{n}_2\sin[\mathbf{Q}_c\cdot\mathbf{r}], \tag{22a}$$

$$\mathbf{S}^c_B(\mathbf{r}) = -\mathbf{n}_1\cos[\mathbf{Q}_c\cdot\mathbf{r} - \Theta(\mathbf{Q}_c)] - \mathbf{n}_2\sin[\mathbf{Q}_c\cdot\mathbf{r} - \Theta(\mathbf{Q}_c)], \tag{22b}$$

where the unit vectors $\mathbf{n}_1$ and $\mathbf{n}_2$ satisfy $\mathbf{n}_1\cdot\mathbf{n}_2 = 0$. The ordering wave vector, $\mathbf{Q}_c$, and the relative phase, $\Theta(\mathbf{Q}_c)$, are defined by the following equations:

$$3 + 2\cos[\mathbf{Q}_c\cdot\mathbf{R}_1] + 2\cos[\mathbf{Q}_c\cdot\mathbf{R}_2] + 2\cos[\mathbf{Q}_c\cdot(\mathbf{R}_1+\mathbf{R}_2)] = (J_2/J_1)^2, \tag{23a}$$

$$(J_2/J_1)e^{i\Theta(\mathbf{Q}_c)} = 1 + e^{i\mathbf{Q}_c\cdot\mathbf{R}_2} + e^{i\mathbf{Q}_c\cdot(\mathbf{R}_1+\mathbf{R}_2)}. \tag{23b}$$

The equations (23) are for the cases of $J_2/J_1 \le 3$. When $J_2/J_1 > 3$, the ground state solution at $J_2/J_1 = 3$ is given for the entire range.

Figure 4 shows the phase diagram obtained by solving the equations (23). In all phases, $\mathbf{Q}_c\cdot\hat{z} = 0$. When $J_2 = 0$, the triangular layers are decoupled and each plane has 120° Néel order with $\mathbf{Q}_c = \pm\mathrm{K} = \pm(\frac{4\pi}{3a}, 0, 0)$ in the first Brillouin zone. Conversely, when $J_2/J_1 \ge 3$, $\mathbf{Q}_c = \mathbf{0}$, and there is inter-plane collinear Néel order. In the intermediate case, $0 \le J_2/J_1 \le 3$, the degenerate spiral ordering wavevectors interpolate between these behaviors, and are shown in Fig. 5.

Throughout our classical Luttinger-Tisza calculations, we find that $\mathbf{Q}_c\cdot\hat{z} = 0$. Hence, for the classical order, we can consider the system as comprised of two layers, which has a honeycomb lattice structure when looked at along the c-axis. Thus, our classical solution is equivalent with those of the J_1-J_2 Heisenberg model on the honeycomb lattice.[23,28]

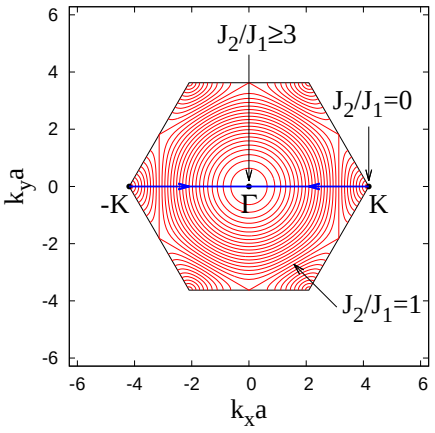

FIG. 5. (Color online) Magnetic ordering wave vectors ($\mathbf{Q}_c$) of the classical solutions. The wave vectors for the degenerate states at a given J_2/J_1 are plotted with a red line in the momentum space, and are determined by (23). The degeneracy is lifted by the quantum order by disorder effect. We show the selected states within the (0,0)-flux ansatz with a blue line, which are described in Sec. VI. The black hexagon denotes the first Brillouin zone at $k_z = 0$.

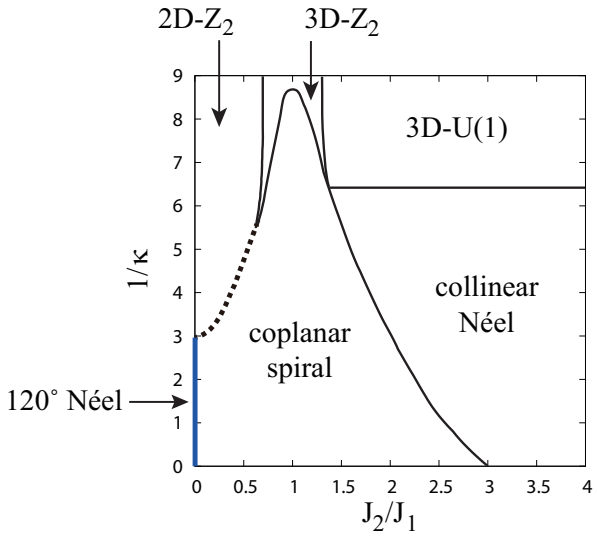

FIG. 6. (Color online) Mean-field phase diagram of the (0,0)-flux ansatz. In the phase diagram, there are three long range orders for large κ, which are the 120° Néel, coplanar spiral, and collinear Néel states, and three spin liquid phases for small κ, which are the $2D$-Z_2, $3D$-Z_2, and $3D$-$U(1)$ states. The thick blue line indicates the region where the 120° Néel state appears. This mean-field phase diagram recovers the classical phases in Fig. 4 in large κ limit. At the boundary between the coplanar spiral and $2D$-Z_2 states (denoted with the dotted line), the phase transition is discontinuous, while a transition at any other phase boundary is continuous.

The classical spiral states for $0 < J_2/J_1 < 3$ spontaneously break lattice rotational symmetry R, as well as spin-rotational symmetry. In the next section, Sec. VI, we will see that the (0,π)-flux ansatz with the full symmetry of the lattice does not host a condensate that gives any such spiral order in the classical limit. In contrast, the (0,0)-flux ansatz does so, and selects the particular states shown in Fig. 5 (blue line).

With the classical limit understood, we now present the phase diagram through the parameter range of quantum fluctuations κ.

VI. MEAN-FIELD PHASE DIAGRAM

In this section, we study the phase diagram for the different ansätze of symmetry groups SG_1 and SG_2, as a function of κ and J_2/J_1, where $\kappa \to \infty$ is the classical limit. As mentioned in previous section, we focus on the (0,0)-flux and (0,π)-flux ansätze among the four ansätze of SG_1. The (π,0)-flux and (π,π)-flux ansätze are discussed in Appendix E, since they always higher mean-field energies, and more importantly they do not reproduce the correct magnetic order in the semi-classical limit.

A. Phase Diagrams for SG_1

1. *(0,0)-flux Ansatz*

The phase diagram for the (0,0)-flux ansatz is given in Fig. 6. In the quantum limit ($\kappa^{-1} \gg 1$), we have three spin liquid phases: the $2D$-Z_2, $3D$-Z_2, and $3D$-$U(1)$ states. In the classical limit ($\kappa^{-1} \ll 1$), there are three long-range orders: the 120° Néel, coplanar spiral, and collinear Néel states. The mean-field parameters of these states are depicted in Fig. 7 and 8 for particular values of κ: $\kappa^{-1} = 9$ for the spin liquid states and $\kappa^{-1} = 1$ for the long-range ordered states. The six phases and the phase transitions among them are discussed below.

a. *$2D$-Z_2 Spin Liquid* In the limit of small J_2/J_1, only the mean-field parameters in the triangular lattice plane, $\eta_{1\alpha}$ and $\eta_{1\beta}$, are non-zero, while the inter-plane parameters $\eta_{2\alpha} = \eta_{2\beta} = 0$. This yields a two-dimensional Z_2 spin liquid. Furthermore, since $\eta_{1\alpha} = \eta_{1\beta}$, it retains the three-fold rotational symmetry, and is in fact one of the bosonic spin liquids on the triangular lattice discovered in earlier studies.[38] The minimum single-spinon gap occurs at the corners of the Brillouin zone, at the points $\pm$K. Furthermore, the Z_2 gauge flux excitations (visons) are also gapped.

b. *$3D$-Z_2 Spin Liquid (nematic spin liquid)* Upon increasing J_2/J_1 further, the inter-plane couplings $\eta_{2\alpha}$ and $\eta_{2\beta}$ become non-zero, along with the intra-plane ones, $\eta_{1\alpha}$ and $\eta_{1\beta}$. Since these parameters all have different magnitudes in general, they break the 120° lattice rotation symmetry. We call such a spin liquid a *nematic* Z_2 spin liquid. As the out-of-plane couplings are also non-zero, this is a gapped three-dimensional

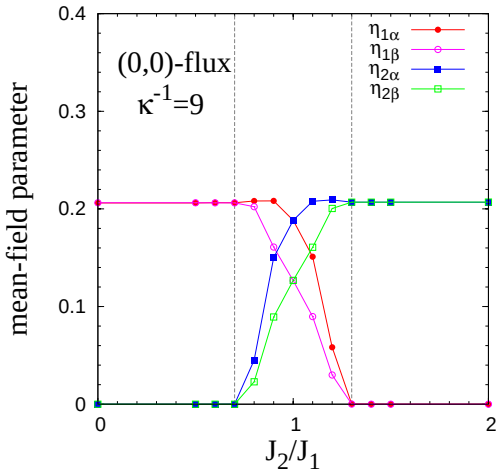

FIG. 7. (Color online) Mean-field parameters of the (0,0)-flux spin liquid states at $\kappa^{-1} = 9$. In the $2D$-Z_2 spin liquid state ($J_2/J_1 \leq 0.7$), $\eta_{1\alpha} = \eta_{1\beta} \neq 0$ and $\eta_{2\alpha} = \eta_{2\beta} = 0$. The opposite is true for the $3D$-$U(1)$ spin liquid state ($J_2/J_1 \geq 1.3$). In the $3D$-Z_2 spin liquid state ($0.7 < J_2/J_1 < 1.3$), every mean-field parameter is nonzero. These features in the mean-field parameters indicate that the $3D$-Z_2 spin liquid state breaks the 120° lattice-rotation symmetry, while the rotation symmetry is preserved in the other two states.

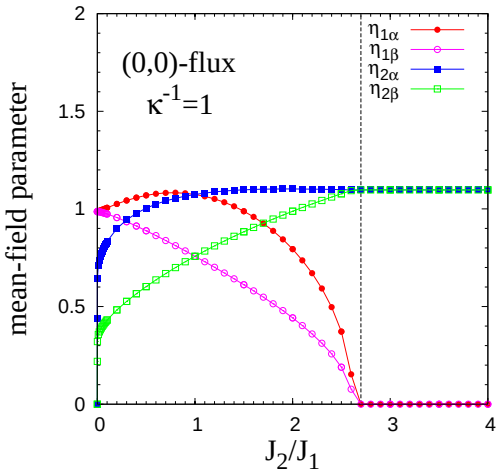

FIG. 8. (Color online) Mean-field parameters of the long-range ordered states in (0,0)-flux ansatz at $\kappa^{-1} = 1$. In the 120° Néel state at $J_2 = 0$, $\eta_{1\alpha} = \eta_{1\beta} \neq 0$ and $\eta_{2\alpha} = \eta_{2\beta} = 0$. The opposite is true for the collinear Néel state when $J_2/J_1 \geq 2.7$. The intermediate coplanar spiral state has a nonzero value for every mean-field parameter.

Z_2 spin liquid. The minimum of the single-spinon gap shifts, from the corners of the Brillouin zone at the ±K points, to the center of an edge of the Brillouin zone at the M point, as J_2/J_1 increases.

c. *3D-U(1) Spin Liquid* When $J_2/J_1 \geq 1.3$ (for instance, at $\kappa^{-1} = 9$), a three-dimensional $U(1)$ spin liquid is stabilized. In this phase, the parameters in the triangular plane are zero, $\eta_{1\alpha} = \eta_{1\beta} = 0$, while the out-of-plane parameters, $\eta_{2\alpha} = \eta_{2\beta} \neq 0$. We immediately notice that the links on which the parameters are non-zero have a bipartite structure. Hence, we can define staggered $U(1)$ transformations of the following form:

$$\begin{aligned} b_{i\mu} &\to e^{i\phi} b_{i\mu} \quad \text{for } i \in \text{A sublattice}, \\ b_{i\mu} &\to e^{-i\phi} b_{i\mu} \quad \text{for } i \in \text{B sublattice}, \end{aligned} \tag{24}$$

for $\phi \in [0, 2\pi)$. In other words, one can assign a positive gauge charge to one sublattice, and a negative gauge charge to the other. This translates into the fact that the IGG is no longer Z_2, but $U(1)$, and we have a three-dimensional $U(1)$ spin liquid. In three dimensions, such a phase may be stabilized, unlike the two-dimensional case. Analysis beyond mean-field shows that low-energy fluctuations of this $U(1)$ spin liquid include two linearly dispersing photons, and hence this phase is gapless.[40–43] The single-spinon gap reaches its minimum at the M point, the center of an edge of the Brillouin zone.

d. *Long-range orders* Upon increasing κ, the spinon gap collapses, and condensation occurs, leading to long-range magnetic order. Depending on the ratio of J_2/J_1, different kinds of magnetic orders are obtained. These are (1) *120° non-collinear Néel order:* at $J_2 = 0$, we have decoupled triangular lattices. For finite but moderate κ ($\gtrsim 1/3$), this supports 120° magnetic order, which is continuously connected to the classical limit. (2) *coplanar spiral order:* on increasing J_2/J_1, the ordering wavevector for the spiral changes, and assumes an incommensurate value, except at special values of J_2/J_1. However, the ordering is coplanar, and the ordering wavevector is in the x-y plane.[28] While the classical solution ($\kappa = \infty$) is degenerate in this regime, at finite κ, a particular ordering wavevector $\mathbf{Q}$ is chosen through quantum order by disorder, as shown in Fig. 5 (blue line). (3) *collinear Néel order:* At large J_2/J_1, the out-of-plane couplings dominate, and since these couplings have a bipartite structure, they stabilize a two-sublattice collinear Néel order. Mean-field parameters for the above long-range ordered states at $\kappa^{-1} = 1$ are plotted in Fig. 8.

Phase Transitions.

In Fig. 6, the transition between the incommensurate spiral and the $2D$-Z_2 spin liquid phases is first-order, while the rest are second order. These second order transitions were studied by Chubukov *et al.*[29] in two dimension. Unlike the usual Landau theory of phase transition, here the coarse grained action is not written in terms of the magnetic order parameter, but in terms of the low-energy spinons $b^\dagger_{i\mu}$, the $U(1)$ gauge field, and the gauge-charge-2 Higgs scalar field η_{ij}. Now, we will briefly describe these transitions. Different phases depend on which of the above bosons are condensed.

1. *Neel - 3D U(1)* : The *collinear Néel phase* is

described as a condensate of the spinons when the gauge-charge-2 Higgs field is gapped. The $U(1)$ gauge field is rendered massive through the Anderson-Higgs mechanism.[29,30] The transition from such a phase to a gapped $U(1)$ spin liquid is obtained by un-condensing the spinons while keeping the charge-2 Higgs field gapped. While this transition is continuous in the mean field level, it is known that fluctuation effects due to the gauge field may render this transition discontinuous in three dimensions.[44]

2. *Neel - Spiral*: In contrast, the transition from the collinear Néel to spiral phase is obtained by condensing the charge-2 Higgs scalar in the background of the spinon condensate.

3. *$U(1)$ - Z_2*: Starting from the $U(1)$ spin liquid, one can condense the charge-2 Higgs scalar, and this breaks down the gauge group from $U(1)$ to Z_2. However, since the spinons are still gapped, this is a Z_2 spin liquid phase.

4. *Z_2 - Spiral*: Finally, the transition from the Z_2 spin liquid to the spiral phase is obtained by condensing the spinons in the background of a charge-2 condensate, thereby completely gapping out the gauge fluctuations.

2. *(0,π)-flux Ansatz*

The phase diagram for the (0,π)-flux phase is shown in Fig. 9. No new phases are present; however, the incommensurate spiral phase at large κ and $3D$-Z_2 spin liquid at small κ are missing in the intermediate J_2/J_1 range.

We note that none of the phases in the phase diagram (Fig. 9) break the lattice rotational symmetry. In addition, the mean-field parameters in the triangular planes are never simultaneously nonzero along with the interplane parameters. At small J_2/J_1, the 120° Néel (at large κ) and $2D$-Z_2 spin liquid (at small κ) phases are found. Upon increasing J_2/J_1, there is a first-order transition into the collinear Néel (at large κ) or $3D$-$U(1)$ spin liquid (at small κ) states. This is unlike the (0,0)-flux phase diagram, where there are intermediate incommensurate spiral and $3D$-Z_2 spin liquid phases. Hence, in the $\kappa \to \infty$ limit, the magnetically ordered phase is not the same for intermediate J_2/J_1 as obtained from the classical analysis.[28]

(0,0)-flux ansatz vs. (0,π)-flux ansatz

Before moving to next subsection, we compare the (0,0)-flux and (0,π)-flux ansätze in terms of the ground state energy and symmetry. Figure 10 shows their ground state energy per site as a function of J_2/J_1 for two particular cases: $\kappa^{-1} = 9$ and $\kappa^{-1} = 1$. The ground state energy per site (ϵ_{gr}) is defined in (D5). From both cases in the figure, it is clearly seen that the (0,0)-flux ansatz (blue) is generally more stable than the (0,π)-flux ansatz (green). In fact, there are two parameter regions where the two ansätze have the same energy: the small J_2/J_1 region and large J_2/J_1 region. In these regions, they have physically identical mean-field solutions, which preserve the lattice-rotation symmetry, in the $2D$-Z_2, $3D$-$U(1)$, 120° Néel, and collinear Néel states. However, when J_1 and J_2 are comparable, two ansätze have different mean-field solutions with different symmetries as discussed in Sec. VI A 1 and VI A 2. In the (0,0)-flux ansatz, the $3D$-Z_2 and coplanar spiral states with broken rotation symmetry are stabilized. However, the (0,π)-flux ansatz allows only the other states with the rotation symmetry. Energetically, the broken symmetry states are more stable than the symmetry-preserving states, as shown in Fig. 10.

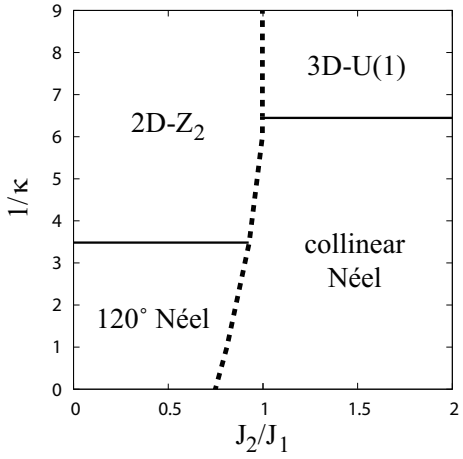

FIG. 9. (Color online) Mean-field phase diagram of the (0,π)-flux ansatz. At small J_2/J_1, the 120° Néel (at small κ^{-1}) and $2D$-Z_2 spin liquid (at large κ^{-1}) phases are found. Upon increasing J_2/J_1, there is a first-order transition (denoted with dotted line) into the collinear Néel (at small κ^{-1}) or $3D$-$U(1)$ spin liquid (at large κ^{-1}) states. The other transitions are second-order. In the phase diagram, every phase preserves the lattice-rotation symmetry, unlike the (0,0)-flux phase diagram in Fig. 6, where there are intermediate phases with broken lattice-rotation symmetry, such as coplanar spiral and $3D$-Z_2 spin liquid states.

From the above energy comparisons, we find that (i) the (0,0)-flux ansatz provides more stable states compared to the (0,π)-flux ansatz and (ii) the system is stabilized by breaking the lattice-rotation symmetry when the system is frustrated due to competing interactions J_1 and J_2.

B. Phase Diagram for SG_2

The phase diagram obtained for the SG_2 ansatz is the same as for the (0,π)-flux ansatz for SG_1, since none of

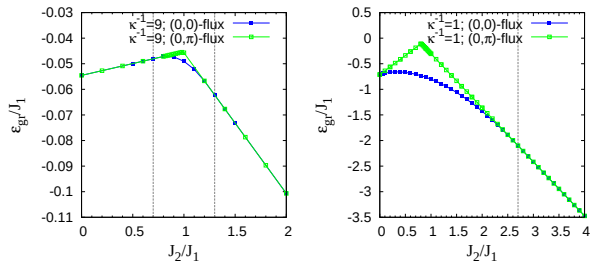

FIG. 10. (Color online) Ground state energy per site (ϵ_{gr}) of the (0,0)-flux and (0,π)-flux ansätze. ϵ_{gr} is defined in (D5). Left: $\kappa^{-1} = 9$ (spin liquid regime). Right: $\kappa^{-1} = 1$ (long-range order regime). The above plots of ϵ_{gr} for both ansätze show that the (0,0)-flux ansatz (blue) is generally more stable than the (0,π)-flux ansatz (green).

the phases obtained break rotational symmetry. Consequently, both of the ansätze have identical mean-field solutions.

VII. TWO-SPINON EXCITATION SPECTRA

Having already discussed the ground state properties of the various spin liquid phases in the previous section, we briefly discuss the two-spinon excitation spectra for various spin liquid states that we find for the (0,0)-flux ansatz with SG_1. Such a two-spinon excitation spectrum is gauge invariant (unlike the spingle spinon spectrum) and is proportional to the spin-structure factor measured in the neutron scattering experiments.[45,46] Hence, it reflects the physical symmetries broken in a phase. In our case, the two-spinon spectrum provides a valuable information for investigating the symmetries of a spin liquid state, especially the broken lattice-rotation symmetry in the nematic spin liquid state.

The lower edge of the two-spinon spectrum is given by[45,46]

$$E_2(\mathbf{k}) = \min_{\mathbf{p}}[\epsilon(\mathbf{p}) + \epsilon(\mathbf{k}-\mathbf{p})], \tag{25}$$

where $\epsilon(\mathbf{k}) = \min\{\omega_1(\mathbf{k}), \cdots, \omega_{n_s}(\mathbf{k})\}$ and $\omega_n(\mathbf{k})$ ($n = 1, \cdots, n_s$) are energy bands of the single-spinon excitations. For more details about $\omega_n(\mathbf{k})$, the reader is referred to Appendix D. $E_2(\mathbf{k})$ of the (0,0)-flux state is plotted in Fig. 11 for several values of J_2/J_1 at $\kappa^{-1} = 9$. The figure clearly shows that the $3D$-Z_2 state breaks the 120° lattice-rotation symmetry, (see (c),(d)) whereas the $2D$-Z_2 and $3D$-$U(1)$ preserve the rotation symmetry (see (b),(e)). In addition, it is observed that $E_2(\mathbf{k})$ continuously changes as J_2/J_1 increases. The $2D$-Z_2 spin liquid state ($J_2/J_1 \leq 0.7$) has the minima of $E_2(\mathbf{k})$ at the $\pm$K points. In the $3D$-Z_2 spin liquid states, ($0.7 < J_2/J_1 < 1.3$) the two minima in the two-spinon spectrum gradually move toward the Γ point as J_2/J_1 increases. When $J_2/J_1 = 1.3$, the two minima merge at the Γ point, which is the minimum of the two-spinon spectrum of the $3D$-$U(1)$ spin liquid ($J_2/J_1 \geq 1.3$). The continuous change in the minimum points is depicted in Fig. 11 (a). The minimum points of each spin liquid state are consistent with the ordering wave vectors of the corresponding long range order state.

The existence of the (0,0)-flux $3D$-Z_2 spin liquid state is an example of a *nematic spin liquid* that breaks the 120° rotational symmetry, but retains time-reversal, spin-rotational, and all other symmetries of the lattice. However, since the spinons may remain in a deconfined phase, such a state retains the fractionalized spin-1/2 excitations and topological order that comprise the exotic behaviours of symmetric spin liquids. Its energetic favorability within mean-field theory, combined with its necessity to describe the spiral order, indicates that such a state may be relevant for a model with the 6H-B structure. Although the Schwinger boson mean-field theory predicts that spiral order is stabilized over a large range of κ, such a nematic spin liquid serves as a starting point for understanding spin-disordered ground states of the frustrated 6H-B structure.

VIII. SUMMARY AND OUTLOOK

In this work, we have analyzed the possible three dimensional bosonic spin liquids on an alternately stacked triangular lattice structure. For the frustrated Heisenberg Hamiltonian with nearest neighbour intra- and inter-plane couplings, we find several three dimensional quantum spin-liquid phases for small values of κ ($\sim 2S$). A central finding of our analysis is a 3D *nematic* Z_2 spin liquid that breaks lattice rotation symmetry that is reflected in the spin-structure factor. Interestingly, our Schwinger boson mean field theory calculation shows that this spin liquid is not only energetically more stable (within self-consistent mean-field theory) than an isotropic one in the same parameter regime, but is also naturally connected to the classical limit of coplanar spiral order. We note that spiral order also breaks lattice rotation symmetries along with spin rotation. It is interesting that this spontaneously broken lattice rotation persists in the nematic spin liquid, even though the spin-rotation invariance is restored across the transition. Though our PSG analysis is aimed to capture Z_2 spin liquids, we identify a bipartite structure of the mean-field parameters in one of the spin liquid phases. The resultant phase actually turns out to be a gapped U(1) spin liquid in three dimensions.

In the present self-consistent mean-field calculations of the given spin-model, the maximum $\kappa \sim 2S$ for which the various spin liquids are stable is rather small compared to the physical value of the spin. However, the spin liquids found here may be stabilized by further neighbour interactions or multi-spin exchange processes for higher values of κ. It would be interesting to see the fate of the nematic spin liquid in such models. Another interesting feature of the phase diagram is the existence of various uncon-

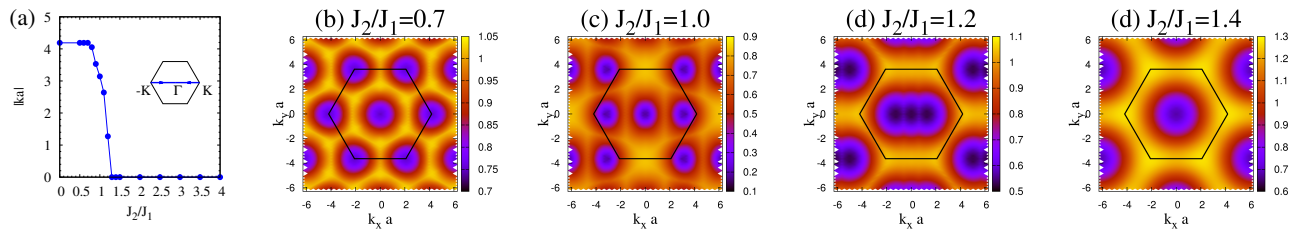

FIG. 11. (Color online) The lower edge of the two-spinon excitations, $E_2(\mathbf{k})/J_1$, of the (0,0)-flux spin liquid states at $\kappa^{-1} = 9$. $E_2(\mathbf{k})$ is defined in (25). We plot the plane $k_z = 0$, which contains the minima of these excitations. (a) The positions of the minima in $E_2(\mathbf{k})$ in the first Brillouin zone as a function of J_2/J_1. (b) The $2D$-Z_2 spin liquid. (c) $\sim$ (d) The $3D$-Z_2 spin liquids. (e) The $3D$-$U(1)$ spin liquid. The two minimum points at $\pm$K gradually move toward the Γ point and then merge at the point as J_2/J_1 increases. In each plot, the hexagon denotes the first Brillouin zone at $k_z = 0$.

ventional quantum phase transitions between the magnetically ordered and disordered phases. Most of these transitions turn out to be continuous within our mean-field theory. We identify these transitions by extending the existing framework[29,30] in terms of condensation of spinons to three spatial dimensions.

It would be interesting to explore, in addition to $Ba_3NiSb_2O_9$, other possible Mott-insulators on three dimensional AB-stacked triangular lattices that may stabilize one or more of the spin liquid phases described here. Of particular interest would be the materials close to metal-insulator transition where charge fluctuations may enhance further neighbour interactions and multi-spin processes.

ACKNOWLEDGMENTS

We thank R. Schaffer for useful discussions. YBK acknowledges the support and hospitality from the Aspen Center for Physics, funded by NSF grant PHY-1066293, and the KITP, funded by NSF grant PHY1125915. This research was supported by the NSERC, CIFAR, and Centre for Quantum Materials at the University of Toronto. The numerical computations were done in SciNet at the University of Toronto.

Appendix A: Projective Symmetry Group Construction I

We split the determination of the PSG into two parts; the first described the procedure and results, leaving most of the details to the second.

In this Appendix, we introduce twenty five multiplication rules among the seven symmetry operations given in (3), construct the PSG corresponding to the three translations, and present the final PSG for both symmetry groups SG_1 and SG_2. We leave the derivation of the PSG elements for the other symmetry group operations to Appendix B.

The multiplication rules among the seven symmetry operations in (3) are given by the following:

$$T_1T_2 = T_2T_1, \tag{A1a}$$
$$T_2T_3 = T_3T_2, \tag{A1b}$$
$$T_1T_3 = T_3T_1, \tag{A1c}$$

$$T_1\Pi_1 = \Pi_1T_1^{-1}, \tag{A2a}$$
$$T_2\Pi_1 = \Pi_1T_1T_2, \tag{A2b}$$
$$T_3\Pi_1 = \Pi_1T_3, \tag{A2c}$$
$$\Pi_1^2 = I, \tag{A2d}$$

$$T_1\Pi_2 = \Pi_2T_1, \tag{A3a}$$
$$T_2\Pi_2 = \Pi_2T_2, \tag{A3b}$$
$$T_3\Pi_2 = \Pi_2T_3^{-1}, \tag{A3c}$$
$$\Pi_2^2 = I, \tag{A3d}$$
$$\Pi_1\Pi_2 = \Pi_2\Pi_1, \tag{A3e}$$

$$T_1\Xi = \Xi T_1^{-1}, \tag{A4a}$$
$$T_2\Xi = \Xi T_2^{-1}, \tag{A4b}$$
$$T_3\Xi = \Xi T_3^{-1}, \tag{A4c}$$
$$\Xi^2 = I, \tag{A4d}$$
$$\Pi_1\Xi = \Xi\Pi_1, \tag{A4e}$$
$$\Pi_2\Xi = \Xi T_3\Pi_2. \tag{A4f}$$

$$T_1R = RT_1^{-1}T_2^{-1}, \tag{A5a}$$
$$T_2R = RT_1, \tag{A5b}$$
$$T_3R = RT_3, \tag{A5c}$$
$$R^3 = I, \tag{A5d}$$
$$R\Pi_1 = \Pi_1R^{-1}, \tag{A5e}$$
$$R\Pi_2 = \Pi_2R, \tag{A5f}$$
$$R\Xi = \Xi T_1^{-1}T_2^{-1}R, \tag{A5g}$$

where I is the identity operator. The above multiplication rules provide constraints on the PSG of the symmetry operations.

We now construct the PSG for the subgroup of translations defined by the equation (A1), re-writing it as

$$T_1^{-1}T_2T_1T_2^{-1} = I, \tag{A6a}$$
$$T_2^{-1}T_3T_2T_3^{-1} = I, \tag{A6b}$$
$$T_1^{-1}T_3T_1T_3^{-1} = I. \tag{A6c}$$

By considering the equivalent expression for PSG elements, as in (15), from (A6a) we obtain

$$\begin{aligned}&(G_{T_1}T_1)^{-1}(G_{T_2}T_2)(G_{T_1}T_1)(G_{T_2}T_2)^{-1}\\ &= (T_1^{-1}G_{T_1}^{-1}T_1)\cdot(T_1^{-1}G_{T_2}T_1)\\ &\quad\cdot((T_1T_2^{-1})^{-1}G_{T_1}(T_1T_2^{-1}))\cdot G_{T_2}^{-1}\\ &\in \mathrm{IGG} = \mathrm{Z}_2,\end{aligned}$$

where G_X $(X = T_1, T_2)$ is the gauge transformation associated with the operation X in the SG. Under G_X, the boson operator acquires the phase $e^{i\phi_X(\mathbf{r})}$. The phase of the above equation can be written as

$$\begin{aligned}&-\phi_{T_1}[T_1(\mathbf{r})] + \phi_{T_2}[T_1(\mathbf{r})]\\ &+\phi_{T_1}[T_1T_2^{-1}(\mathbf{r})] - \phi_{T_2}[\mathbf{r}] = n_1\pi,\end{aligned} \tag{A7}$$

where $n_1 \in \{0, 1\}$ and $n_1 = 0$ $(n_1 = 1)$ corresponds to the element $+1$ (-1) in the Z_2 gauge group. Equation (A7) is the first constraint on the PSG. Whenever we derive a constraint on the PSG from a multiplication rule among the symmetry operations, we employ an integer variable, like n_1 in the above equation. Hereafter, n_i $(i = 1, \cdots, 25)$ is regarded as an integer variable, which is either 0 or 1. It must be noted that in all phase equations like (A7), equality is to be understood as modulo 2π, due to the 2π periodicity in the phases.

Determining the possible solutions of the constraint equations like (A7) can be facilitated by an appropriate choice of gauge fixing. For the first gauge fixing, we set

$$\phi_{T_1}(r_1, r_2, r_3)_p = 0, \tag{A8}$$

for both sublattices $(p = A, B)$. Then, (A7) is reduced to

$$\phi_{T_2}(r_1, r_2, r_3)_p = \phi_{T_2}(0, r_2, r_3)_p + n_1\pi r_1. \tag{A9}$$

Taking another gauge fixing

$$\phi_{T_2}(0, r_2, r_3)_p = 0, \tag{A10}$$

we obtain

$$\phi_{T_2}(r_1, r_2, r_3)_p = n_1\pi r_1. \tag{A11}$$

In a similar way, $\phi_{T_3}(\mathbf{r})$ is determined from (A6b) and (A6c). If we use (A8) and (A11) and take the gauge-fixing

$$\phi_{T_3}(0, 0, r_3)_p = 0, \tag{A12}$$

then we are lead to

$$\phi_{T_3}(r_1, r_2, r_3)_p = n_2\pi r_2 + n_3\pi r_1. \tag{A13}$$

We must ensure to fix the gauge freedom so as to satisfy (A8), (A10), (A12) at the same time. The gauge-fixings can be realized in the following way.[51] Suppose that $\phi_{T_n}^{(0)}$ $(n = 1, 2, 3)$ is the initial choice for the phase of G_{T_n}. Then, we consider a series of gauge transformations G_m $(m = 1, 2, 3)$, so that

$$\phi_{T_n}^{(0)} \xrightarrow{G_1} \phi_{T_n}^{(1)} \xrightarrow{G_2} \phi_{T_n}^{(2)} \xrightarrow{G_3} \phi_{T_n}^{(3)}, \tag{A14a}$$

where $G_m = e^{i\phi_{G_m}}$ $(m = 1, 2, 3)$ is defined as follows:

$$\begin{aligned}\phi_{G_m}(r_1, r_2, r_3)_p = &-\sum_{i=-\infty}^{r_1}\phi_{T_1}^{(m-1)}(i, r_2, r_3)_p\\ &-\sum_{j=-\infty}^{r_2}\phi_{T_2}^{(m-1)}(0, j, r_3)_p\\ &-\sum_{k=-\infty}^{r_3}\phi_{T_3}^{(m-1)}(0, 0, k)_p.\end{aligned} \tag{A14b}$$

It is important to note that ϕ_{G_m} depends on $\phi_{T_n}^{(m-1)}$. To determine $\phi_{T_n}^{(m)}$ $(m = 1, 2, 3)$, it is necessary to understand how an arbitrary gauge transformation changes G_X. It can be understood from the fact that our mean-field ansatz is invariant under the PSG, $\{G_XX\}$. Then, if we take a gauge transformation G, the transformed mean-field ansatz is invariant under $G\cdot G_XX\cdot G^{-1} = \tilde{G}_X\cdot X$, where $\tilde{G}_X = G\cdot G_X\cdot XG^{-1}X^{-1}$. This gives us a new PSG, $\{\tilde{G}_X\cdot X\}$. Then, under the transformation G, $\phi_X[\mathbf{r}]$ changes in following way.

$$\phi_X[\mathbf{r}] \xrightarrow{G} \phi_G[\mathbf{r}] + \phi_X[\mathbf{r}] - \phi_G[X^{-1}(\mathbf{r})]. \tag{A15}$$

According to above transformation rule, $\phi_X[\mathbf{r}]$ acquires the additional phase $\phi_G[\mathbf{r}] - \phi_G[X^{-1}(\mathbf{r})]$ under the transformation G. Applying the above rule to each transformation in (A14), we find that the gauge fixings (A8), (A10), (A12) are all satisfied. As seen in the definition of (A14), the above gauge-fixing is defined for open boundary conditions. Periodic boundary conditions introduce additional subtleties, so we consider the PSG for systems with open boundary conditions, with the understanding that the particular boundary condition will be irrelevant in the thermodynamic limit.

Readers who are interested in detailed derivation of G_X for the rest of the symmetry group are referred to Appendix B. We present the phases ϕ_X of G_X for the full PSG below.

PSG for SG_1:

$$\phi_{T_{1,3}}(r_1, r_2, r_3)_p = 0, \tag{A16a}$$
$$\phi_{T_2}(r_1, r_2, r_3)_p = n_1\pi r_1, \tag{A16b}$$
$$\phi_{\Pi_1}(r_1, r_2, r_3)_p = \left(\frac{1}{2} + \delta_{p,B}\right)\pi - \frac{1}{2}n_1\pi r_2(r_2 - 1), \tag{A16c}$$
$$\phi_{\Pi_2}(r_1, r_2, r_3)_p = 0, \tag{A16d}$$
$$\phi_{\Xi}(r_1, r_2, r_3)_p = \frac{\pi}{2} + n_1\pi r_1, \tag{A16e}$$

where $n_1 = 0, 1$.

Considering the remaining rotation R, we obtain the PSG for the SG_2. The rotational symmetry leads to $n_1 = 0$ in (A16) as shown in Appendix B 4.

PSG for SG_2:

$$\phi_{T_{1,2,3}}(r_1, r_2, r_3)_p = 0, \tag{A17a}$$
$$\phi_{\Pi_1}(r_1, r_2, r_3)_p = \left(\frac{1}{2} + \delta_{p,B}\right)\pi, \tag{A17b}$$
$$\phi_{\Pi_2}(r_1, r_2, r_3)_p = 0, \tag{A17c}$$
$$\phi_{\Xi}(r_1, r_2, r_3)_p = \frac{\pi}{2}, \tag{A17d}$$
$$\phi_{R}(r_1, r_2, r_3)_p = 0. \tag{A17e}$$

Appendix B: Projective Symmetry Group Construction II

In this section, we derive the transformation $G_X = e^{i\phi_X}$ for the remaining elements of SG_1 and SG_2 beyond the translations.

1. $\phi_{\Pi_1}(r_1, r_2, r_3)_p$

Rewriting (A2) into constraints like (A7), and solving the resultant equations, we obtain

$$\begin{aligned}&\phi_{\Pi_1}(r_1, r_2, r_3)_p \\ &= \phi_{\Pi_1}(0,0,0)_p + n_4\pi r_1 + n_5\pi r_2 + n_6\pi r_3 \\ &- \frac{n_1}{2}\pi r_2(r_2 - 1) - n_3\pi r_2 r_3,\end{aligned} \tag{B1}$$

and

$$2\phi_{\Pi_1}(0,0,0)_p = n_7\pi, \tag{B2a}$$
$$n_4 = 0. \tag{B2b}$$

Of the above equations, (B1) is determined by (A2a,b,c) and (B2) by (A2d). As mentioned earlier, integer variables (n_i) are introduced when multiplication rules among the symmetry operations are used to place a constraint on the PSG. In the above expressions, the integer variable n_5 can be eliminated by the gauge transformation $G_4 = e^{i\phi_{G_4}}$, where

$$\phi_{G_4}(r_1, r_2, r_3)_p = \pi r_1.$$

Under this transformation,

$$\phi_{T_n}(r_1, r_2, r_3)_p \to \phi_{T_n}(r_1, r_2, r_3)_p + \delta_{n,1}\pi \ (n = 1, 2, 3),$$
$$\phi_{\Pi_1}(r_1, r_2, r_3)_p \to \phi_{\Pi_1}(r_1, r_2, r_3)_p - \pi r_2.$$

In fact, the additional constant $\delta_{n,1}\pi$ in ϕ_{T_n} can be ignored since we may add a site-independent constant π to ϕ_X because IGG=Z_2. So the gauge transformation does not change ϕ_{T_n} $(n = 1, 2, 3)$. As for ϕ_{Π_1}, if $n_5 = 1$, $n_5\pi r_2$ in (B1) is removed under the transformation. Combining the above results with (A8), (A11), (A13), the PSG for $\{T_1, T_2, T_3, \Pi_1\}$ is described as follows:

$$\begin{aligned}\phi_{T_1}(r_1, r_2, r_3)_p &= 0, \\ \phi_{T_2}(r_1, r_2, r_3)_p &= n_1\pi r_1, \\ \phi_{T_3}(r_1, r_2, r_3)_p &= n_2\pi r_2 + n_3\pi r_1, \\ \phi_{\Pi_1}(r_1, r_2, r_3)_p &= \phi_{\Pi_1}(0,0,0)_p + n_6\pi r_3 \\ &\quad - \frac{1}{2}n_1\pi r_2(r_2 - 1) - n_3\pi r_2 r_3,\end{aligned}$$

where

$$2\phi_{\Pi_1}(0,0,0)_p = n_7\pi.$$

2. $\phi_{\Pi_2}(r_1, r_2, r_3)_p$

Conducting similar calculations as above for (A3) leads to the following equations:

$$\begin{aligned}\phi_{\Pi_2}(r_1, r_2, r_3)_p &= \phi_{\Pi_2}(0,0,0)_p \\ &\quad + n_8\pi r_1 + n_9\pi r_2 + n_{10}\pi r_3,\end{aligned} \tag{B3}$$
$$2\phi_{\Pi_2}(0,0,0)_p = (n_{10}\cdot\delta_{p,B} + n_{11})\pi, \tag{B4}$$
$$n_3 = n_6 = n_8 = n_{12} = 0. \tag{B5}$$

(B3) is determined by (A3a,b,c), (B4) by (A3d), and (B5) by (A3e). Using this result, the PSG for $\{T_1, T_2, T_3, \Pi_1, \Pi_2\}$ is given by

$$\begin{aligned}\phi_{T_1}(r_1, r_2, r_3)_p &= 0, \\ \phi_{T_2}(r_1, r_2, r_3)_p &= n_1\pi r_1, \\ \phi_{T_3}(r_1, r_2, r_3)_p &= n_2\pi r_2, \\ \phi_{\Pi_1}(r_1, r_2, r_3)_p &= \phi_{\Pi_1}(0,0,0)_p - \frac{1}{2}n_1\pi r_2(r_2 - 1), \\ \phi_{\Pi_2}(r_1, r_2, r_3)_p &= \phi_{\Pi_2}(0,0,0)_p + n_9\pi r_2 + n_{10}\pi r_3,\end{aligned}$$

where

$$\begin{aligned}2\phi_{\Pi_1}(0,0,0)_p &= n_7\pi, \\ 2\phi_{\Pi_2}(0,0,0)_p &= (n_{10}\cdot\delta_{p,B} + n_{11})\pi.\end{aligned}$$

3. $\phi_{\Xi}(r_1, r_2, r_3)_p$

Repeating the same procedure for (A4), we obtain

$$\begin{aligned}\phi_{\Xi}(r_1, r_2, r_3)_p &= \phi_{\Xi}(0,0,0)_p \\ &\quad + n_{13}\pi r_1 + n_{14}\pi r_2 + n_{15}\pi r_3,\end{aligned} \tag{B6}$$
$$\phi_{\Xi}(0,0,0)_p + \phi_{\Xi}(0,0,0)_{\bar{p}} = n_{16}\pi, \tag{B7}$$

$$n_1 = n_{13}, \tag{B8a}$$
$$\phi_{\Pi_1}(0,0,0)_B = \phi_{\Pi_1}(0,0,0)_{\bar{p}} + n_{17}\pi, \tag{B8b}$$

and

$$n_2 = n_{10} = n_{15} = 0, \tag{B9a}$$
$$\phi_{\Pi_2}(0,0,0)_B = \phi_{\Pi_2}(0,0,0)_A + n_{18}\pi. \tag{B9b}$$

The first equation (B6) is determined by (A4a,b,c), (B7) by (A4d), (B8) by (A4e), and (B9) by (A4f). Now we have the PSG for $\{T_1, T_2, T_3, \Pi_1, \Pi_2, \Xi\}$, which is described by

$$\begin{aligned}
\phi_{T_{1,3}}(r_1,r_2,r_3)_p &= 0,\\
\phi_{T_2}(r_1,r_2,r_3)_p &= n_1\pi r_1,\\
\phi_{\Pi_1}(r_1,r_2,r_3)_p &= \phi_{\Pi_1}(0,0,0)_p - \frac{1}{2}n_1\pi r_2(r_2-1),\\
\phi_{\Pi_2}(r_1,r_2,r_3)_p &= \phi_{\Pi_2}(0,0,0)_p, +n_9\pi r_2,\\
\phi_{\Xi}(r_1,r_2,r_3)_p &= \phi_{\Xi}(0,0,0)_p, +n_1\pi r_1 + n_{14}\pi r_2,
\end{aligned}$$

where

$$\begin{aligned}
2\phi_{\Pi_1}(0,0,0)_p &= n_7\pi,\\
2\phi_{\Pi_2}(0,0,0)_p &= n_{11}\pi,\\
\phi_{\Xi}(0,0,0)_A + \phi_{\Xi}(0,0,0)_B &= n_{16}\pi,\\
\phi_{\Pi_1}(0,0,0)_B &= \phi_{\Pi_1}(0,0,0)_A + n_{17}\pi.\\
\phi_{\Pi_2}(0,0,0)_B &= \phi_{\Pi_2}(0,0,0)_A + n_{18}\pi.
\end{aligned}$$

There are eight integer variables in the PSG obtained above. However, in determining possible mean-field Hamiltonians, most of those variables can be eliminated by using symmetries. To be specific, we assume

$$\eta_{(0,0,0)_A\to(1,0,0)_A} \neq 0, \tag{B10a}$$
$$\eta_{(0,0,0)_A\to(0,1,0)_A} \neq 0, \tag{B10b}$$
$$\eta_{(0,0,0)_A\to(0,0,0)_B} \neq 0, \tag{B10c}$$
$$\eta_{(0,0,0)_A\to(1,1,0)_B} \neq 0. \tag{B10d}$$

It must be noted that the above four mean-field parameters are independent because they can not be transformed to each other via any symmetry operation in SG_1. (This fact will be used when we construct the mean-field ansätze in Appendix C). Applying the equation (14) to the above nonzero mean-field parameters, we can find additional constraints on the eight integer variables and then obtain (A16). First, we simplify ϕ_Π. Noting that the link $(0,0,0)_A \to (0,0,0)_B$ does not move under the operation Π_1 and using the equation (14) with $X = \Pi_1$, $i = (0,0,0)_A$, $j = (0,0,0)_B$, we have

$$\phi_{\Pi_1}(0,0,0)_A + \phi_{\Pi_1}(0,0,0)_B = 0. \tag{B11}$$

Next, we note that for both of the sublattice $p = A, B$,

$$\begin{aligned}
&(-1,0,0)_p \to (0,0,0)_p \xrightarrow{T_1} (0,0,0)_p \to (1,0,0)_p\\
&\xrightarrow{\Pi_1} (0,0,0)_p \to (-1,0,0)_p = -(-1,0,0)_p \to (0,0,0)_p.
\end{aligned}$$

In this case, the equation (14) is written as follows:

$$\begin{aligned}
&-\eta_{(-1,0,0)_p\to(0,0,0)_p}\\
&= \eta_{(0,0,0)_p\to(1,0,0)_p}\cdot e^{-i\phi_{\Pi_1}[\Pi_1(0,0,0)_p]-i\phi_{\Pi_1}[\Pi_1(1,0,0)_p]}\\
&= \eta_{(-1,0,0)_p\to(0,0,0)_p}\cdot e^{-i\phi_{\Pi_1}[\Pi_1(0,0,0)_p]-i\phi_{\Pi_1}[\Pi_1(1,0,0)_p]},
\end{aligned}$$

where we used $\phi_{T_1} = 0$. The above equation is reduced to

$$\phi_{\Pi_1}[\Pi_1(0,0,0)_p] + \phi_{\Pi_1}[\Pi_1(1,0,0)_p] = \pi.$$

Simplifying the above equation, we get the condition

$$\begin{aligned}
&2\phi_{\Pi_1}(0,0,0)_p = \pi \ (p = A, B) \qquad \text{(B12)}\\
&\Rightarrow n_7 = 1.
\end{aligned}$$

Subtracting (B11) from (B12), we find one more condition:

$$\begin{aligned}
&\phi_{\Pi_1}(0,0,0)_B - \phi_{\Pi_1}(0,0,0)_A = \pi \qquad \text{(B13)}\\
&\Rightarrow n_{17} = 1.
\end{aligned}$$

Then, $\phi_{\Pi_1}(0,0,0)_p$ is determined by (B11), (B12), and (B13):

$$\phi_{\Pi_1}(0,0,0)_p = \left(\frac{1}{2} + m_1 + \delta_{p,B}\right)\pi,$$

where $m_1 \in \{0,1\}$. Ignoring the constant $m_1\pi$ (because IGG=Z_2), we obtain (A16c).

Next, to simplify ϕ_{Π_2}, we notice that the link $(0,0,0)_A \to (1,0,0)_A$ is invariant under Π_2. From this fact,

$$\begin{aligned}
&\phi_{\Pi_2}(0,0,0)_A + \phi_{\Pi_2}(1,0,0)_A = 0\\
&\Rightarrow 2\phi_{\Pi_2}(0,0,0)_A = 0\\
&\Rightarrow n_{11} = 0,
\end{aligned}$$

Then, we have $2\phi_{\Pi_2}(0,0,0)_p = n_{11}\pi = 0$ $(p = A, B)$, from which $\phi_{\Pi_2}(0,0,0)_p$ can be written as

$$\phi_{\Pi_2}(0,0,0)_p = (m_2 + m_3\cdot\delta_{p,B})\pi,$$

where $m_2, m_3 \in \{0,1\}$. Considering another link invariant under Π_2, $(0,0,0)_A \to (0,1,0)_A$, we get additional constraint:

$$\begin{aligned}
&\phi_{\Pi_2}(0,0,0)_A + \phi_{\Pi_2}(0,1,0)_A = 0\\
&\Rightarrow 2\phi_{\Pi_2}(0,0,0)_A + n_9\pi = 0\\
&\Rightarrow n_9 = 0.
\end{aligned}$$

With above conditions, ϕ_{Π_2} can be written as

$$\begin{aligned}
\phi_{\Pi_2}(r_1,r_2,r_3)_p &= \phi_{\Pi_2}(0,0,0)_p\\
&= (m_2 + m_3\cdot\delta_{p,B})\pi. \qquad \text{(B14)}
\end{aligned}$$

ϕ_{Π_2} can be simplified further by taking following gauge transformation $G_5 = e^{i\phi_5}$:

$$\phi_5(r_1,r_2,r_3)_p = \pi r_3.$$

Under the transformation, only ϕ_{Π_2} is affected as follows.

$$\phi_{\Pi_2}(r_1,r_2,r_3)_p \to \phi_{\Pi_2}(r_1,r_2,r_3)_p + \pi\cdot\delta_{p,B}.$$

With this transformation, $\delta_{p,B}\cdot m_3\pi$ in (B14) can be eliminated. Ignoring $m_2\pi$ in the equation as well (IGG=Z_2), the equation is reduced to (A16d).

Finally, we simplify ϕ_Ξ. Let us consider the link $(0,0,0)_A \to (0,0,0)_B$.

$$\begin{aligned}
&(0,0,0)_A \to (0,0,0)_B \xrightarrow{\Xi} (0,0,0)_B \to (0,0,0)_A\\
&= -(0,0,0)_A \to (0,0,0)_B.
\end{aligned}$$

From this, we obtain

$$\begin{aligned}&\phi_\Xi(0,0,0)_A+\phi_\Xi(0,0,0)_B=\pi\\ \Rightarrow\ & n_{16}=1.\end{aligned}\tag{B15}$$

We also note that

$$\begin{aligned}&(-1,-1,0)_A\to(0,0,0)_B\xrightarrow{T_1T_2}(0,0,0)_A\to(1,1,0)_B\\ \xrightarrow{\Xi}\ &(0,0,0)_B\to(-1,-1,0)_A=-(-1,-1,0)_A\to(0,0,0)_B.\end{aligned}$$

It follows that

$$\begin{aligned}&[\phi_{T_2}(-1,-1,0)_A+\phi_{T_2}(0,0,0)_B]\\ +\ &[\phi_\Xi(0,0,0)_A+\phi_\Xi(1,1,0)_B]=\pi\\ \Rightarrow\ &\phi_\Xi(0,0,0)_A+\phi_\Xi(0,0,0)_B+n_{14}\pi=\pi\\ \Rightarrow\ &n_{14}=0.\end{aligned}\tag{B16}$$

From the conditions (B15) and (B16), ϕ_Ξ can be written as follows:

$$\phi_\Xi(r_1,r_2,r_2)_p=\phi_\Xi(0,0,0)_p+n_1\pi r_1,$$

where

$$\phi_\Xi(0,0,0)_p=\begin{cases}\phi_0 & (p=A)\\ \pi-\phi_0 & (p=B)\end{cases}.$$

The dependence of ϕ_Ξ on the sublattice can be eliminated by the gauge transformation $G_6=e^{i\phi_{G_6}}$, where

$$\phi_6(r_1,r_2,r_3)_p=\begin{cases}\phi_1 & (p=A)\\ -\phi_1 & (p=B)\end{cases}.$$

Under the transformation, only ϕ_Ξ changes, in the following way:

$$\phi_\Xi(r_1,r_2,r_3)_p\to\phi_\Xi(r_1,r_2,r_3)_p+2\phi_1\cdot(-1)^{\delta_{p,B}}.$$

By choosing $2\phi_1=\pi/2-\phi_0$, we obtain

$$\phi_\Xi(r_1,r_2,r_3)_p=\frac{\pi}{2}+n_1\pi r_1,$$

which is same as (A16e).

4. $\phi_R(r_1,r_2,r_3)_p$

We now consider adding the rotation R to the symmetry group, in order to find the PSGs for SG_2. We obtain following conditions from (A5a,b,c).

$$\begin{aligned}&\phi_R(r_1,r_2,r_3)_p\\ =\ &\phi_R(0,0,0)_p+n_{19}\pi r_1+n_{20}\pi r_2+n_{21}\pi r_3\\ +\ &n_1\pi r_1r_2-\frac{1}{2}n_1\pi r_1(r_1-1).\end{aligned}\tag{B17}$$

From (A5d), we get two conditions:

$$n_{21}=0,\tag{B18a}$$
$$3\phi_R(0,0,0)_p=n_{22}\pi-(n_1+n_{19})\pi\cdot\delta_{p,B}.\tag{B18b}$$

By using the constraint from (A5e),

$$n_1=n_{19}+n_{20},\tag{B19a}$$
$$2\phi_R(0,0,0)_p=n_{23}\pi.\tag{B19b}$$

Using the conditions (B18) and (B19), we can simplify (B17) as follows.

$$\begin{aligned}\phi_R(r_1,r_2,r_3)_p=\ &\phi_R(0,0,0)_p+n_{19}\pi r_1+n_{20}\pi r_2\\ &+n_1\pi r_1r_2-\frac{1}{2}n_1\pi r_1(r_1-1),\end{aligned}\tag{B20}$$

where

$$\begin{aligned}&n_1=n_{19}+n_{20},\\ &\phi_R(0,0,0)_p=(n_{22}+n_{23})\pi+n_{20}\pi\cdot\delta_{p,B}.\end{aligned}\tag{B21}$$

The equation (A5f,g) does not give a new condition on the integer variables.

The above expression for ϕ_R can be further simplified by using rotational symmetries for certain links. First, we note that

$$\begin{aligned}(0,0,0)_A\to(1,1,0)_B\xrightarrow{R}\ &(0,0,0)_A\to(0,1,0)_B\\ \xrightarrow{\Pi_1}\ &(0,0,0)_A\to(1,1,0)_B.\end{aligned}$$

Applying (14) to the above relation,

$$\begin{aligned}&\phi_R(0,0,0)_A+\phi_R(0,0,0)_B=0\\ \Rightarrow\ &n_{20}=0\Rightarrow n_{19}=n_1.\end{aligned}\tag{B22}$$

The last equation is obtained from the fact that $n_1=n_{19}+n_{20}$. Next, we consider following symmetry:

$$\begin{aligned}&(1,0,0)_A\to(1,1,0)_A\xrightarrow{R}(0,1,0)_A\to(-1,0,0)_A\\ \xrightarrow{\Pi_1}\ &(1,1,0)_A\to(1,0,0)_A=-(1,0,0)_A\to(1,1,0)_A.\end{aligned}$$

For this case, (14) gives us

$$\begin{aligned}&[\phi_R(1,0,0)_A+\phi_R(1,1,0)_A]\\ +\ &[\phi_{\pi_1}(0,1,0)_A+\phi_{\pi_1}(-1,0,0)_A]=\pi\\ \Rightarrow\ &n_1=0.\end{aligned}\tag{B23}$$

Plugging the conditions (B22) and (B23) into (B20) and (B21), we have following expression for ϕ_R:

$$\phi_R(r_1,r_2,r_3)_p=(n_{22}+n_{23})\pi.\tag{B24}$$

It must be remembered that the site-independent constant $(n_{22}+n_{23})\pi$ in the equation can be ignored due to IGG=Z_2. The conditions (B23) and (B24) lead to (A17), the PSG for the SG_2.

Appendix C: Brief sketch of the derivation of mean-field ansätze

In this section, we construct the ansätze of the SG_1. To find out the possible ansätze for a given symmetry group, we must classify all possible projective symmetry groups. In the PSG for the SG_1 (A16), there is only

one integer variable: $n_1 = 0, 1$. Different values of n_1 correspond to distinct PSGs. However, there is another factor to determine the PSGs in addition to n_1, which is the relative sign between the four independent mean-field parameters (B10). We assume that the mean-field parameters is real-valued to preserve the time reversal symmetry. Then, they can be positive or negative. However, we can fix three of those parameters to be positive in a certain orientation by employing several gauge transformations below.

First, the mean-field parameter $\eta_{(0,0,0)_A\to(1,0,0)_A}$ can be fixed to be positive via the transformation $G_7 = e^{i\phi_7}$, where

$$\phi_7(r_1, r_2, r_3)_p = \text{constant}. \tag{C1}$$

Next, we can render the parameter $\eta_{(0,0,0)_A\to(0,1,0)_A}$ positive by using the transformation $G_8 = e^{i\phi_8}$, where

$$\phi_8(r_1, r_2, r_3)_p = \pi r_2. \tag{C2}$$

Finally, the parameter $\eta_{(0,0,0)_A\to(0,0,0)_B}$ becomes positive in the help of the transformation $G_9 = e^{i\phi_9}$ with

$$\phi_9(r_1, r_2, r_3)_p = \pi \cdot \delta_{p,A}. \tag{C3}$$

Under the transformations (C1), (C2), (C3), the PSGs (A16) and (A17) are invariant up to a constant π, which can be ignored due to IGG=Z_2. Therefore, the parameter $\eta_{(0,0,0)_A\to(1,1,0)_B}$ is only free to change its sign. Now, we define positive mean-field parameters ($\eta_{1\alpha}$, $\eta_{1\beta}$, $\eta_{2\alpha}$, $\eta_{2\beta}$) as follows:

$$\begin{aligned}
\eta_{(0,0,0)_A\to(1,0,0)_A} &\equiv \eta_{1\alpha}, && \text{(C4a)}\\
\eta_{(0,0,0)_A\to(0,1,0)_A} &\equiv \eta_{1\beta}, && \text{(C4b)}\\
\eta_{(0,0,0)_A\to(0,0,0)_B} &\equiv \eta_{2\alpha}, && \text{(C4c)}\\
\eta_{(0,0,0)_A\to(1,1,0)_B} &\equiv \eta_{2\beta}\cdot(-1)^m, && \text{(C4d)}
\end{aligned}$$

where $m = 0, 1$. The integer variable m is the other factor to determine the ansätze in addition to n_1. Therefore, there are four distinct ansätze corresponding to four different combinations of n_1 and m. The four ansätze are classified in Table I.

Now we construct the mean-field ansätze for the symmetry group SG_1. The ansätze are constructed by using (14) and (A16). This generates the values of all symmetry-related mean-field parameters from a single bond, through the application of elements of the PSG.

1. $(0,\pi)$-flux and $(0,0)$-flux ansätze

First, we consider the cases of $n_1 = 0$. If we set $X = T_n$ ($n = 1, 2, 3$) in (14) and use (A16a) and (A16b) with $n_1 = 0$, then we have

$$\eta_{T_n(i)T_n(j)} = \eta_{ij}.$$

This means that the mean-field ansätze with $n_1 = 0$ are translationally invariant. Therefore, it is enough to specify the mean-field structure within a unit cell for the ansätze.

Considering the unit cell denoted with the ellipse in Fig. 1, the twelve links consist of six intra-layer links (C5) and six inter-layer links (C6).

$$\begin{aligned}
&(0,0,0)_A \to (1,0,0)_A, && \text{(C5a)}\\
&(0,0,0)_A \to (0,1,0)_A, && \text{(C5b)}\\
&(0,0,0)_A \to (1,1,0)_A, && \text{(C5c)}\\
&(0,0,0)_B \to (-1,0,0)_B, && \text{(C5d)}\\
&(0,0,0)_B \to (0,-1,0)_B, && \text{(C5e)}\\
&(0,0,0)_B \to (-1,-1,0)_B, && \text{(C5f)}
\end{aligned}$$

$$\begin{aligned}
&(0,0,0)_A \to (0,0,0)_B, && \text{(C6a)}\\
&(0,0,0)_A \to (1,1,0)_B, && \text{(C6b)}\\
&(0,0,0)_A \to (0,1,0)_B, && \text{(C6c)}\\
&(0,0,0)_A \to (0,0,-1)_B, && \text{(C6d)}\\
&(0,0,0)_A \to (1,1,-1)_B, && \text{(C6e)}\\
&(0,0,0)_A \to (0,1,-1)_B. && \text{(C6f)}
\end{aligned}$$

We fix mean-field parameters at four links, (C5a), (C5b), (C6a), and (C6b) , as mentioned in (C4). The links (C5) and (C6) within the unit cell are connected by symmetry operations of SG_1 toin following way.

$$\begin{array}{ccc}
\boxed{\text{(C5a)}} & \boxed{\text{(C5b)}} & \xrightarrow{\Pi_1} \text{(C5c)}\\
\Xi\downarrow & \Xi\downarrow & \Xi\downarrow\\
\text{(C5d)} & \text{(C5e)} & \xrightarrow{\Pi_1} \text{(C5f)}
\end{array}$$

$$\begin{array}{ccc}
\boxed{\text{(C6a)}} & \boxed{\text{(C6b)}} & \xrightarrow{\Pi_1} \text{(C6c)}\\
\Pi_2\downarrow & \Pi_2\downarrow & \Pi_2\downarrow\\
\text{(C6d)} & \text{(C6e)} & \xrightarrow{\Pi_1} \text{(C6f)}
\end{array} \tag{C7}$$

In the above diagram, the boxes denote the links where the mean-field parameter is fixed. If we apply (14) to (C7), we can determine the other eight mean-field parameters in the unit cell. Their mean-field configurations in the unit cell are given as follows.

$$\begin{aligned}
\eta_{1\alpha} &= \eta_{(0,0,0)_A\to(1,0,0)_A} = \eta_{(-1,0,0)_B\to(0,0,0)_B},\\
\eta_{1\beta} &= \eta_{(0,0,0)_A\to(0,1,0)_A} = \eta_{(1,1,0)_A\to(0,0,0)_A}\\
&= \eta_{(0,-1,0)_B\to(0,0,0)_B} = \eta_{(0,0,0)_B\to(-1,-1,0)_B},\\
\eta_{2\alpha} &= \eta_{(0,0,0)_A\to(0,0,0)_B} = \eta_{(0,0,0)_A\to(0,0,-1)_B},\\
(-1)^m\cdot\eta_{2\beta} &= \eta_{(0,0,0)_A\to(1,1,0)_B} = \eta_{(0,0,0)_A\to(1,1,-1)_B}\\
&= \eta_{(0,0,0)_A\to(0,1,0)_B} = \eta_{(0,0,0)_A\to(0,1,-1)_B}.
\end{aligned}$$

Here, the case of $m = 1$ corresponds to (0,0)-flux ansatz and $m = 0$ does to $(0,\pi)$-flux ansatz. The mean-field configuration in a unit cell of the (0,0)-flux ansatz is depicted in Fig. 12. Switching the positive orientation of $\eta_{2\beta}$ in the figure leads to the $(0,\pi)$-flux ansatz.

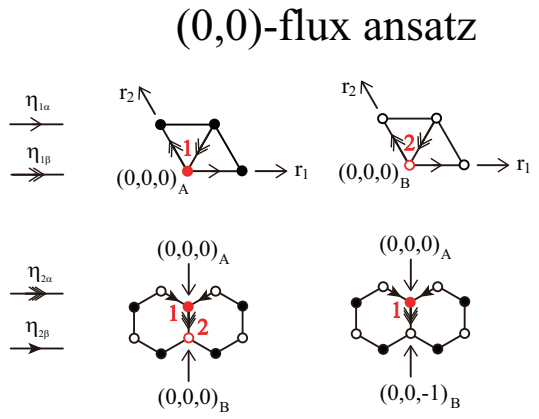

FIG. 12. (Color online) (0,0)-flux ansatz. The figure shows the two sites (red and numbered) and the twelve mean-fields (arrowed links) in a unit cell. The full mean-field configuration is obtained via translations along the three lattice vectors $\{\mathbf{R}_1, \mathbf{R}_2, \mathbf{R}_3\}$. Switching the positive orientation of $\eta_{2\beta}$ in the figure leads to the (0,π)-flux ansatz.

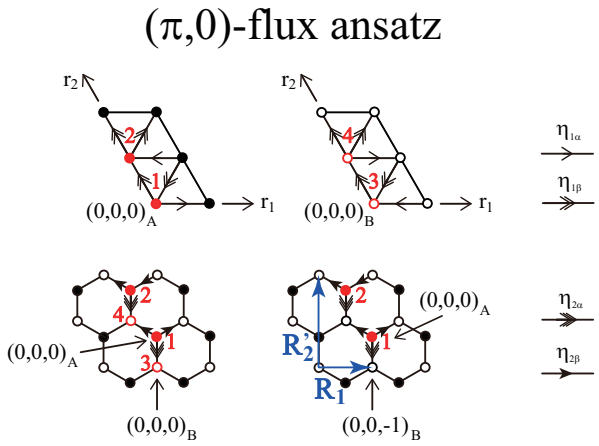

FIG. 13. (Color online) (π,0)-flux ansatz. The figure shows the four sites (red and numbered) and the twenty four mean-fields (arrowed links) in a unit cell. The ansatz has the orthorhombic Bravais lattice structure. The lattice vectors of the orthorhombic lattice are given by $\{\mathbf{R}_1, \mathbf{R}_2', \mathbf{R}_3\}$, where $\mathbf{R}_2' = \mathbf{R}_1 + 2\mathbf{R}_2$. The full mean-field configuration is obtained via translations along the three lattice vectors. Switching the positive orientation of $\eta_{2\beta}$ in the figure leads to the (π,π)-flux ansatz.

2. $(\pi, 0)$-flux and (π, π)-flux ansätze

Repeating the same procedure above for the cases of $n_1 = 1$, we can obtain following ansätze.

$$
\begin{aligned}
\eta_{1\alpha} &= \eta_{(0,0,0)_A\to(1,0,0)_A} = \eta_{(1,1,0)_A\to(0,1,0)_A} \\
&= \eta_{(1,0,0)_B\to(0,0,0)_B} = \eta_{(0,1,0)_B\to(1,1,0)_B}, \\
\eta_{1\beta} &= \eta_{(0,0,0)_A\to(0,1,0)_A} = \eta_{(0,1,0)_A\to(0,2,0)_A} \\
&= \eta_{(1,1,0)_A\to(0,0,0)_A} = \eta_{(0,1,0)_A\to(1,2,0)_A} \\
&= \eta_{(0,0,0)_B\to(0,1,0)_B} = \eta_{(0,1,0)_B\to(0,2,0)_B} \\
&= \eta_{(1,1,0)_B\to(0,0,0)_B} = \eta_{(0,1,0)_B\to(1,2,0)_B}, \\
\eta_{2\alpha} &= \eta_{(0,0,0)_A\to(0,0,0)_B} = \eta_{(0,1,0)_A\to(0,1,0)_B} \\
&= \eta_{(0,0,0)_A\to(0,0,-1)_B} = \eta_{(0,1,0)_A\to(0,1,-1)_B}, \\
(-1)^m\cdot\eta_{2\beta} &= \eta_{(0,0,0)_A\to(1,1,0)_B} = \eta_{(0,0,0)_A\to(0,1,0)_B} \\
&= \eta_{(0,1,0)_A\to(0,2,0)_B} = \eta_{(1,2,0)_B\to(0,1,0)_A} \\
&= \eta_{(0,0,0)_A\to(1,1,-1)_B} = \eta_{(0,0,0)_A\to(0,1,-1)_B} \\
&= \eta_{(0,1,0)_A\to(0,2,-1)_B} = \eta_{(1,2,-1)_B\to(0,1,0)_A}.
\end{aligned}
$$

The two ansätze have enlarged unit cell because ϕ_{T_2} is site-dependent when $n_1 = 1$ [see (A16b)]. There are four sites and twenty four links in a unit cell. The case of $m = 0$ corresponds to (π,0)-flux ansatz and $m = 1$ does to (π,π)-flux ansatz. Fig. 13 shows the mean-field configuration in a unit cell of the (π,0)-flux ansatz. The configuration for the (π,π)-flux ansatz is obtained by switching the positive orientation of $\eta_{2\beta}$ in the figure.

3. Symmetric ansatz

The symmetric ansatz with the full symmetry group SG_2 can be constructed by considering the constraints due to the rotational symmetry: $n_1 = 0$, $m = 0$, and $\eta_{1\alpha} = \eta_{1\beta}$ and $\eta_{2\alpha} = \eta_{2\beta}$. The condition $n_1 = 0$ was already found in Section B 4. The rest of the conditions come from the fact that $\phi_R = 0$ in (A17). Therefore, the symmetric ansatz is a special case of the (0,π)-flux ansatz with $\eta_{1\alpha} = \eta_{1\beta}$ and $\eta_{2\alpha} = \eta_{2\beta}$.

Appendix D: Mean-field Hamiltonians

In this appendix, we provide the mean-field Hamiltonians of the ansätze obtained in previous section in momentum space. For each ansatz, the mean-field Hamiltonian takes the following form:

$$H_{MF} = N_{uc}\cdot n_s\cdot\epsilon_0 + \sum_{\mathbf{k}}\Psi^\dagger(\mathbf{k})\mathbf{D}(\mathbf{k})\Psi(\mathbf{k}), \quad \text{(D1)}$$

where

$$
\begin{aligned}
\epsilon_0 &= -\lambda(\kappa+1) \\
&\quad + \sum_{n=1}^{2} J_n\left(\frac{1}{2}|\eta_{n\alpha}|^2 + |\eta_{n\beta}|^2 + \frac{3}{4}\kappa^2\right),
\end{aligned}
$$

$$\Psi(\mathbf{k}) = (b_{1\uparrow}(\mathbf{k}),\cdots,b_{n_s\uparrow}(\mathbf{k}), b^\dagger_{1\downarrow}(-\mathbf{k}),\cdots,b^\dagger_{n_s\downarrow}(-\mathbf{k}))^T,$$

$$\mathbf{D}(\mathbf{k}) = \left(\begin{array}{c|c} \lambda\mathbb{I}_{n_s} & \mathbf{F}(\mathbf{k}) \\ \hline \mathbf{F}^\dagger(\mathbf{k}) & \lambda\mathbb{I}_{n_s}\end{array}\right).$$

In the above expressions, N_{uc} is the number of unit cells and n_s is the number of sites in a unit cell. The (0,0)-flux and (0,π)-flux ansätze have $n_s = 2$ and the (π,0)-flux and (π,π)-flux ansätze have $n_s = 4$. $b_{n\mu}(\mathbf{k})$ ($n = 1,\cdots,n_s; \mu = \uparrow,\downarrow$) is the boson operator in momentum

l	l'	$\mathbf{R}$	$J_{ll'}(\mathbf{R})$	$\eta_{ll'}(\mathbf{R})$
1	1	$\mathbf{R}_1$	J_1	$\eta_{1\alpha}$
1	1	$\mathbf{R}_2$	J_1	$\eta_{1\beta}$
1	1	$-\mathbf{R}_1-\mathbf{R}_2$	J_1	$\eta_{1\beta}$
2	2	$\mathbf{R}_1$	J_1	$\eta_{1\alpha}$
2	2	$\mathbf{R}_2$	J_1	$\eta_{1\beta}$
2	2	$-\mathbf{R}_1-\mathbf{R}_2$	J_1	$\eta_{1\beta}$
1	2	$\mathbf{0}$	J_2	$\eta_{2\alpha}$
1	2	$\mathbf{R}_1+\mathbf{R}_2$	J_2	$(-1)^m\cdot\eta_{2\beta}$
1	2	$\mathbf{R}_2$	J_2	$(-1)^m\cdot\eta_{2\beta}$
1	2	$-\mathbf{R}_3$	J_2	$\eta_{2\alpha}$
1	2	$\mathbf{R}_1+\mathbf{R}_2-\mathbf{R}_3$	J_2	$(-1)^m\cdot\eta_{2\beta}$
1	2	$\mathbf{R}_2-\mathbf{R}_3$	J_2	$(-1)^m\cdot\eta_{2\beta}$

TABLE II. $J_{ll'}(\mathbf{R})$ and $\eta_{ll'}(\mathbf{R})$ in (D2) for the (0,0)-flux and (0,π)-flux ansätze. The case of $m=1$ corresponds to the (0,0)-flux ansatz and $m=0$ does to the (0,π)-flux ansatz.

space. The subscript n denotes the site in a unit cell and the site-numbering is shown in Fig. 12 and 13 (red numbers). λ is the Lagrange multiplier, which is taken to be uniform. $\mathbb{I}_{n_s}$ is the $n_s\times n_s$ identity matrix. The other $n_s\times n_s$ matrix $\mathbf{F}(\mathbf{k})$ are defined as follows:

$$\begin{aligned}\mathbf{F}_{nn'}(\mathbf{k}) = &-\frac{1}{2}\sum_{(l,l',\mathbf{R})\in \mathrm{L}} J_{ll'}(\mathbf{R})\eta_{ll'}(\mathbf{R})\cdot e^{i\mathbf{k}\cdot\mathbf{R}}\cdot\delta_{nl}\delta_{n'l'}\\ &+\frac{1}{2}\sum_{(l,l',\mathbf{R})\in \mathrm{L}} J_{ll'}(\mathbf{R})\eta_{ll'}(\mathbf{R})\cdot e^{-i\mathbf{k}\cdot\mathbf{R}}\cdot\delta_{nl'}\delta_{n'l},\end{aligned} \tag{D2}$$

where the set L and $J_{ll'}(\mathbf{R})$ and $\eta_{ll'}(\mathbf{R})$ are listed in Table II and III.

The mean-field Hamiltonian (D1) is diagonalized via the Bogoliubov transformation:[52]

$$\Psi(\mathbf{k}) = \mathbf{M}(\mathbf{k})\Gamma(\mathbf{k}),$$

where

$$\Gamma(\mathbf{k}) = (\gamma_{1\uparrow}(\mathbf{k}),\cdots,\gamma_{n_s\uparrow}(\mathbf{k}),\gamma^\dagger_{1\downarrow}(-\mathbf{k}),\cdots,\gamma^\dagger_{n_s\downarrow}(-\mathbf{k}))^T.$$

$\gamma_{l\alpha}(\mathbf{k})$ satisfies the bosonic statistics, which imposes a condition on the transformation matrix $\mathbf{M}(\mathbf{k})$:

$$\mathbf{M}(\mathbf{k})\mathbb{I}_B\mathbf{M}^\dagger(\mathbf{k}) = \mathbb{I}_B, \tag{D3}$$

where

$$\mathbb{I}_B = \left(\begin{array}{c|c} \mathbb{I}_{n_s} & 0 \\ \hline 0 & -\mathbb{I}_{n_s}\end{array}\right).$$

Due to this constraint, $\mathbb{I}_B\mathbf{D}(\mathbf{k})$ is diagonalized instead of $\mathbf{D}(\mathbf{k})$, so the eigenvalue problem has the following form:

$$\mathbf{M}^{-1}(\mathbf{k})\mathbb{I}_B\mathbf{D}(\mathbf{k})\mathbf{M}(\mathbf{k}) = \mathbb{I}_B\mathbf{\Omega}(\mathbf{k}),$$

where $\mathbf{\Omega}(\mathbf{k})$ is the diagonal matrix of eigenvalues,

$$\mathbf{\Omega}(\mathbf{k}) = \mathrm{diag}(\omega_{1\uparrow}(\mathbf{k}),\cdots,\omega_{n_s\uparrow}(\mathbf{k}),\omega_{1\downarrow}(-\mathbf{k}),\cdots,\omega_{n_s\downarrow}(-\mathbf{k})),$$

l	l'	$\mathbf{R}$	$J_{ll'}(\mathbf{R})$	$\eta_{ll'}(\mathbf{R})$
1	1	$\mathbf{R}_1$	J_1	$\eta_{1\alpha}$
1	2	$\mathbf{0}$	J_1	$\eta_{1\beta}$
2	1	$-\mathbf{R}_1$	J_1	$\eta_{1\beta}$
2	2	$-\mathbf{R}_1$	J_1	$\eta_{1\alpha}$
2	1	$-\mathbf{R}_1+\mathbf{R}'_2$	J_1	$\eta_{1\beta}$
2	1	$\mathbf{R}'_2$	J_1	$\eta_{1\beta}$
3	3	$-\mathbf{R}_1$	J_1	$\eta_{1\alpha}$
3	4	$\mathbf{0}$	J_1	$\eta_{1\beta}$
4	3	$-\mathbf{R}_1$	J_1	$\eta_{1\beta}$
4	2	$\mathbf{R}_1$	J_1	$\eta_{1\alpha}$
4	3	$-\mathbf{R}_1+\mathbf{R}'_2$	J_1	$\eta_{1\beta}$
4	3	$\mathbf{R}'_2$	J_1	$\eta_{1\beta}$
1	3	$\mathbf{0}$	J_2	$\eta_{2\alpha}$
1	4	$\mathbf{R}_1$	J_2	$(-1)^m\cdot\eta_{2\beta}$
1	4	$\mathbf{0}$	J_2	$(-1)^m\cdot\eta_{2\beta}$
2	4	$\mathbf{0}$	J_2	$\eta_{2\alpha}$
3	2	$-\mathbf{R}'_2$	J_2	$(-1)^m\cdot\eta_{2\beta}$
2	3	$-\mathbf{R}_1+\mathbf{R}'_2$	J_2	$(-1)^m\cdot\eta_{2\beta}$
1	3	$-\mathbf{R}_3$	J_2	$\eta_{2\alpha}$
1	4	$\mathbf{R}_1-\mathbf{R}_3$	J_2	$(-1)^m\cdot\eta_{2\beta}$
1	4	$-\mathbf{R}_3$	J_2	$(-1)^m\cdot\eta_{2\beta}$
2	4	$-\mathbf{R}_3$	J_2	$\eta_{2\alpha}$
3	2	$-\mathbf{R}'_2+\mathbf{R}_3$	J_2	$(-1)^m\cdot\eta_{2\beta}$
2	3	$-\mathbf{R}_1+\mathbf{R}'_2-\mathbf{R}_3$	J_2	$(-1)^m\cdot\eta_{2\beta}$

TABLE III. $J_{ll'}(\mathbf{R})$ and $\eta_{ll'}(\mathbf{R})$ in (D2) for the (π,0)-flux and (π,π)-flux ansätze. The case of $m=0$ corresponds to the (π,0)-flux ansatz and $m=1$ does to the (π,π)-flux ansatz.

In fact, $\omega_{l\uparrow}(\mathbf{k}) = \omega_{l\downarrow}(-\mathbf{k}) \equiv \omega_l(\mathbf{k})$ ($l=1,\cdots,n_s$), due to the time reversal symmetry of the mean-field Hamiltonian. In addition, $\omega_l(\mathbf{k}) = \omega_l(-\mathbf{k})$ since $\mathbf{D}(-\mathbf{k}) = \mathbf{D}^*(\mathbf{k})$. The eigenvectors are contained in the columns of $\mathbf{M}(\mathbf{k})$ and normalized according to (D3). By the above transformation,

$$H_{MF} = N_{uc}\cdot n_s\cdot\epsilon_{gr} + \sum_{\mathbf{k}}\sum_{l=1}^{n_s}\omega_l(\mathbf{k})\gamma^\dagger_{l\alpha}(\mathbf{k})\gamma_{l\alpha}(\mathbf{k}),$$

where ϵ_{gr} is the ground state energy per site;

$$\epsilon_{gr} = \epsilon_0 + \frac{1}{N_{uc}\cdot n_s}\sum_{\mathbf{k}}\sum_{l=1}^{n_s}\omega_l(\mathbf{k}). \tag{D4}$$

The single-spinon excitation spectrum is given by $\omega_l(\mathbf{k})$.

If the spinon excitation becomes gapless at $\mathbf{k}=\pm\mathbf{k}^*$, then the spinon condensate is considered:

$$\begin{aligned}\mathbf{x}(\mathbf{k}) &= \langle\Psi(\mathbf{k})\rangle\\ &\equiv \left(x_{1\uparrow}(\mathbf{k}),\cdots,x_{n_s\uparrow}(\mathbf{k}),x^*_{1\downarrow}(-\mathbf{k}),\cdots,x^*_{n_s\downarrow}(-\mathbf{k})\right)^T.\end{aligned}$$

In the existence of the condensate, the ground state energy is modified into following form:

$$\begin{aligned}\epsilon_{gr} = \epsilon_0 &+ \frac{1}{N_{uc}\cdot n_s}\sum_{\mathbf{k}\neq\pm\mathbf{k}^*}\sum_{l=1}^{n_s}\omega_l(\mathbf{k})\\ &+ \frac{1}{N_{uc}\cdot n_s}\sum_{\mathbf{k}=\pm\mathbf{k}^*}\mathbf{x}^\dagger(\mathbf{k})\mathbf{D}(\mathbf{k})\mathbf{x}(\mathbf{k}).\end{aligned} \tag{D5}$$

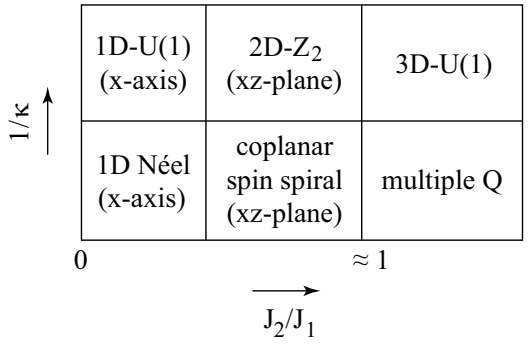

FIG. 14. Schematic phase diagram of the $(\pi,0)$-flux and (π,π)-flux ansätze.

The condensate vector is a zero-energy eigenvector found from

$$\mathbf{D}(\pm\mathbf{k}^*)\mathbf{x}(\pm\mathbf{k}^*)=0, \tag{D6a}$$

where $\mathbf{x}(\pm\mathbf{k}^*)$ is normalized to satisfy

$$\kappa=\sum_{\mathbf{k}=\pm\mathbf{k}^*}\sum_{l=1}^{n_s}x^*_{l\mu}(\mathbf{k})x_{l\mu}(\mathbf{k}) + \sum_{\mathbf{k}\neq\pm\mathbf{k}^*}\sum_{l=1}^{n_s}\langle b^\dagger_{l\mu}(\mathbf{k})b_{l\mu}(\mathbf{k})\rangle. \tag{D6b}$$

Then, the ground state is determined by solving

$$\frac{\partial\epsilon_{gr}}{\partial\eta}=0\ (\eta=\eta_{1\alpha},\cdots,\eta_{2\beta}), \tag{D6c}$$

together with (D6a) and (D6b). (D6) is the momentum space version of the self-consistent mean-field equations (9).

Appendix E: Mean-field phase diagrams of $(\pi,0)$-flux and (π,π)-flux ansätze

In this appendix, we present the results of the mean-field theories for the $(\pi,0)$-flux and (π,π)-flux ansätze. As will be shown below, the ansätze are energetically less favoured (within SBMFT) than the (0,0)-flux and (0,π)-flux ansätze. Moreover, the semi-classical limit of the $(\pi,0)$-flux and (π,π)-flux ansätze does not recover the classical spin states found in Sec. V.

1. $(\pi,0)$-flux ansatz

Figure 14 shows a schematic phase diagram for the $(\pi,0)$-flux ansatz. In the quantum limit ($\kappa^{-1}\gg1$), there are three spin liquid phases: the $1D$-$U(1)$, $2D$-Z_2, and $3D$-$U(1)$ states. In the semi-classical limit ($\kappa^{-1}\ll1$), we find three different kinds of long-range orders: the 1D Néel, spin spiral, and multiple $\mathbf{Q}$ states. The detailed analysis of the phase boundaries are complicated due to the presence of multiple minima in the spinon band structure and hence we only discuss the schematic phase diagram. For the spin liquid states, the mean-field parameters are depicted in Fig. 15 for $\kappa^{-1}=5$. The lower bound two-spinon dispersion for each spin liquid state is plotted in Fig. 16.

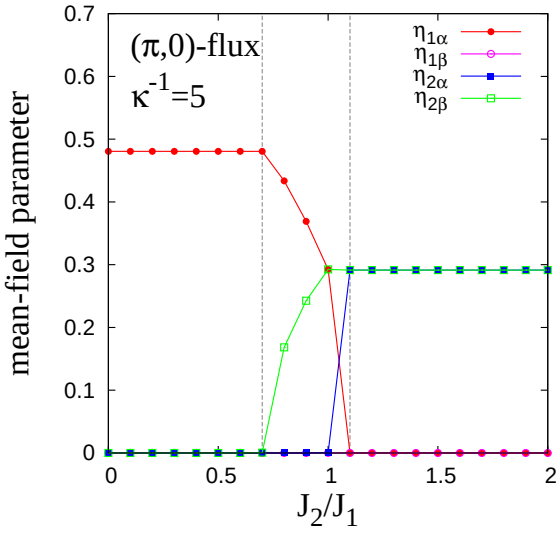

FIG. 15. (Color online) Mean-field parameters of the $(\pi,0)$-flux spin liquid states at $\kappa^{-1}=5$. In the plot, $\eta_{2\alpha}$ is all the way zero.

a. *$1D$-$U(1)$ Spin Liquid* In the limit of small J_2/J_1, only $\eta_{1\alpha}$ is nonzero and the other parameters are all zero. This leads to an one-dimensional spin liquid along the x axis or r_1 direction. The minimum of the single-spinon gap occurs at the points $(\pm\frac{\pi}{2a},0,0)$. Particularly, the 1D spin liquid is stabilized even at the point $J_2=0$, where the system is reduced to stacked and decoupled 2D triangular lattices.This is in contrast to the natural expectation of recovering the π-flux state[38] in the 2D triangular lattice limit, just like we obtained the 0-flux state of the triangular lattice in the $J_2=0$ limit of the (0,0)-flux and (0,π)-flux ansätze in Sec. VI. In the present case, we however, find that the π-flux state ($\eta_{1\alpha}=\eta_{1\beta}$) is not the global energy minimum in the space of the parameters $\{\eta_{1\alpha},\ \eta_{1\beta}\}$ (see in Fig. 17). We think that this $1D-U(1)$ spin liquid is an artifact of our mean field theory and it is unstable to other phases. Based on previous analysis[38], the π-flux state appears to be a good candidate phase in this regime. However, a more systematic treatment of this parameter regime is required.

b. *$2D$-Z_2 Spin Liquid* Upon increasing J_2/J_1 further, $\eta_{2\beta}$ becomes nonzero in addition to $\eta_{1\alpha}$. However, $\eta_{1\beta}$ and $\eta_{2\alpha}$ remain zero. Considering the links of $\eta_{1\alpha}$ and $\eta_{2\beta}$, one can find that the links has the 2D anisotropic triangular lattice structure along the xz-plane or r_1r_3-plane. This yields a $2D$-Z_2 spin liquid state. This spin liquid state is gauge-equivalent to the 0-flux state of the anisotropic triangular lattice.[38,46] In particular, when

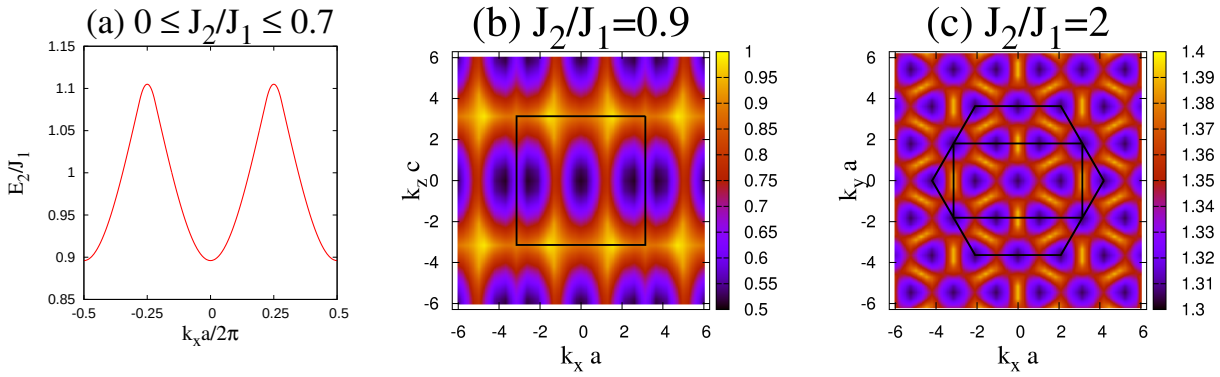

FIG. 16. (Color online) The lower edge of the two-spinon excitations, $E_2(\mathbf{k})/J_1$, of the $(\pi,0)$-flux spin liquid states at $\kappa^{-1}=5$. $E_2(\mathbf{k})$ is defined in (25). (a) The $1D$-$U(1)$ spin liquid along the x-axis. (b) The $2D$-Z_2 spin liquid along the xz-plane. The rectangle denotes the first Brillouin zone of the ansatz in the k_xk_z-plane. (c) The $3D$-$U(1)$ spin liquid. In this case, we plot $E_2(\mathbf{k})$ in the plane $k_z=0$ where the minima of the two-spinon excitation occur. The hexagon denotes the first Brillouin zone of the 6H-B lattice structure and the rectangle does the Brillouin zone of the ansatz.

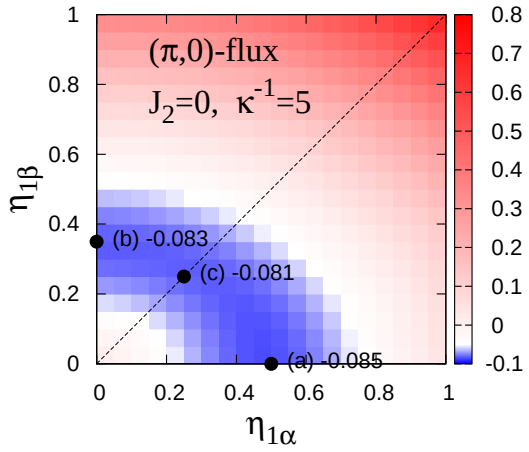

FIG. 17. (Color online) Plot of energy (ϵ_{gr}/J_1) as a function of $\{\eta_{1\alpha},\eta_{1\beta}\}$ for the $(\pi,0)$-flux ansatz at $J_2=0$ and $\kappa^{-1}=5$. Three dots denote the local extrema (the figure indicates the energy at each point). (a) The energy minimum point: the $1D$-$U(1)$ spin liquid. (b) A local minimum point. (c) A saddle point lying on the line $\eta_{1\alpha}=\eta_{1\beta}$: the π-flux spin liquid state in the 2D triangular lattice.[38]

$J_2/J_1=1$, the 0-flux spin liquid state of the isotropic triangular lattice is obtained (see $\eta_{1\alpha}=\eta_{2\beta}$ at $J_2/J_1=1$ in Fig. 15). The $2D$-Z_2 spin liquid state has the lowest single-spinon excitations at (±q,0,0).

c. $3D$-$U(1)$ *Spin Liquid* In the limit of large J_2/J_1, $\eta_{1\alpha}$ vanishes and $\eta_{2\alpha}$ has the same magnitude as $\eta_{2\beta}$. $\eta_{1\beta}$ still remains zero. The mean-field links of $\{\eta_{2\alpha},\eta_{2\beta}\}$ have a three-dimensional, honeycomb-like bipatite lattice structure. The resulting state is a $3D$-$U(1)$ spin liquid state. The lowest spinon excitations appear at the four points: $\pm(\frac{1}{12}\mathbf{G}_1+\frac{1}{4}\mathbf{G}_2)$ and $\pm(\frac{5}{12}\mathbf{G}_1+\frac{1}{4}\mathbf{G}_2)$, where $\mathbf{G}_1=(\frac{2\pi}{a},0,0)$, $\mathbf{G}_2=(0,\frac{2\pi}{\sqrt{3}a},0)$, and $\mathbf{G}_3=(0,0,\frac{2\pi}{c})$. $\{\mathbf{G}_n\}_{n=1}^3$ are the reciprocal lattice vectors of the lattice vectors $\{\mathbf{R}_1,\mathbf{R}_2^{'},\mathbf{R}_3\}$.

d. *Long-range orders* In large κ limit, spinons are condensed at the minima of the spinon dispersion and a magnetic long-range order is developed. We find three kinds of magnetic orders. (1) *1D Néel order*: when $J_2/J_1\ll 1$, the one-dimensional Néel state is stabilized with the ordering wave vector $\pm(\frac{\pi}{a},0,0)$. (2) *Coplanar spin spiral order*: on increasing J_2/J_1, neighboring 1D Néel spin chains are correlated along the xz-plane and the coplanar spin spiral order is developed along the plane. The ordering wave vectors are given by $\pm(Q,0,0)$ ($Q<\frac{\pi}{a}$). (3) *Multiple-***Q** *state*: when $J_2/J_1>1$, we find magnetic state with multiple ordering wave vectors (**Q**). The multiple ordering wave vectors result from the spinon condensation at the four points, $\pm(\frac{1}{12}\mathbf{G}_1+\frac{1}{4}\mathbf{G}_2)$ and $\pm(\frac{5}{12}\mathbf{G}_1+\frac{1}{4}\mathbf{G}_2)$, in the $3D$-$U(1)$ spin liquid. The wave vectors can be identified with the positions of the two-spinon dispersion minima in Fig. 16 (c). The details of the complicated magnetic structure is presently not understood.

2. (π,π)-flux ansatz

The overall phase diagram of the (π,π)-flux ansatz has the same structure as that of the $(\pi,0)$-flux ansatz. We find a difference between the two ansätze in the region of the multiple **Q** state: they have gauge-inequivalent mean-field states. In the other regions, their mean-field states are gauge-equivalent.

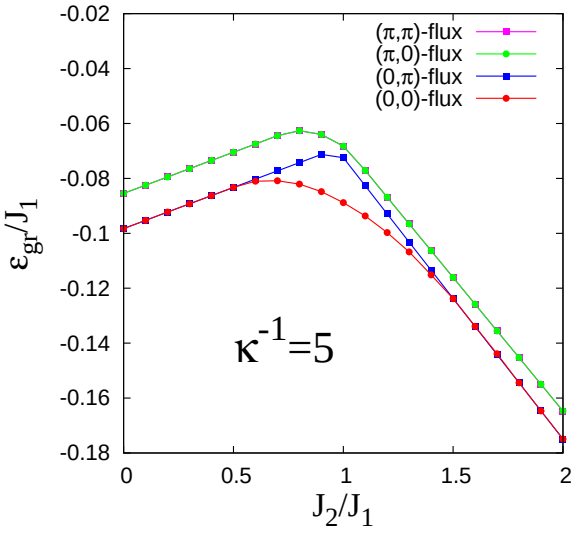

FIG. 18. (Color online) Energy comparison among the ansätze with the symmetry group SG_1. The (0,0)-flux ansatz is the most stable among the ansätze with the symmetry group SG_1. The (π,0)-flux and (π,π)-flux ansätze have the same energy since they have gauge-equivalent mean-field states.

3. Mean-field Energy comparison

We close this appendix with an energy comparison (obtained from our SBMFT) among the ansätze of SG_1. Fig. 18 shows the ground state energy of each ansatz at $\kappa^{-1} = 5$. The (π,0)-flux and (π,π)-flux ansätze have higher energies than the (0,0)-flux ansatz, which is the most stable among the ansätze with the symmetry group SG_1. We find that this pattern is true for general κ^{-1}. In the figure, the (π,0)-flux and (π,π)-flux ansätze have the same energies since their mean-field states are gauge-equivalent.

[1] P. W. Anderson, Mat. Res. Bull. **8**, 153 (1973).
[2] X.-G. Wen, Phys. Rev. B **65**, 165113 (2002).
[3] A. Kitaev, Ann. Phys. **321**, 2 (2006).
[4] P. A. Lee, Sciene **321**, 1306 (2008).
[5] L. Balents, Nature (London) **464**, 199 (2010).
[6] S. Yan, D. A. Huse, and S. R. White, Science **332**, 1173 (2011).
[7] H.-C. Jiang, H. Yao, and L. Balents, Phys. Rev. B **86**, 024424 (2012).
[8] H.-C. Jiang, Z. Wang, and L. Balents, Nat. Phys. **8**, 902 (2012).
[9] Y. Shimizu, K. Miyagawa, K. Kanoda, M. Maesato, and G. Saito, Phys. Rev. Lett. **91**, 107001 (2003).
[10] R. Coldea, D. A. Tennant, and Z. Tylczynski, Phys. Rev. B **68**, 134424 (2003).
[11] S. Yamashita, T. Yamamoto, Y. Nakazawa, M. Tamura, and R. Kato, Nat. Commun. **2**, 275 (2011).
[12] P. Mendels, F. Bert, M. A. de Vries, A. Olariu, A. Harrison, F. Duc, J. C. Trombe, J. S. Lord, A. Amato, and C. Baines, Phys. Rev. Lett. **98**, 077204 (2007).
[13] J. S. Helton, K. Matan, M. P. Shores, E. A. Nytko, B. M. Bartlett, Y. Yoshida, Y. Takano, A. Suslov, Y. Qiu, J.-H. Chung, D. G. Nocera, and Y. S. Lee, Phys. Rev. Lett. **98**, 107204 (2007).
[14] T. Han, S. Chu, and Y. S. Lee, Phys. Rev. Lett. **108**, 157202 (2012).
[15] Y. Okamoto, M. Nohara, H. Aruga-Katori, and H. Takagi, Phys. Rev. Lett. **99**, 137207 (2007).
[16] K. A. Ross, L. Savary, B. D. Gaulin, and L. Balents, Phys. Rev. X **1**, 021002 (2011).
[17] H. D. Zhou, E. S. Choi, G. Li, L. Balicas, C. R. Wiebe, Y. Qiu, J. R. D. Copley, and J. S. Gardner, Phys. Rev. Lett. **106**, 147204 (2011).
[18] S. Nakatsuji, K. Kuga, K. Kimura, R. Satake, N. Katayama, E. Nishibori, H. Sawa, R. Ishii, M. Hagiwara, and F. Bridges, Science **336**, 559 (2012).
[19] J. A. Quilliam, F. Bert, E. Kermarrec, C. Payen, C. Guillot-Deudon, P. Bonville, C. Baines, H. Luetkens, and P. Mendels, Phys. Rev. Lett. **109**, 117203 (2012).
[20] J. G. Cheng, G. Li, L. Balicas, J. S. Zhou, J. B. Goodenough, C. Xu, and H. D. Zhou, Phys. Rev. Lett. **107**, 197204 (2011).
[21] M. Serbyn, T. Senthil, and P. A. Lee, Phys. Rev. B **84**, 180403(R) (2011).
[22] C. Xu, F. Wang, Y. Qi, L. Balents, and M. P. A. Fisher, Phys. Rev. Lett. **108**, 087204 (2012).
[23] G. Chen, M. Hermele, and L. Radzihovsky, Phys. Rev. Lett. **109**, 016402 (2012).
[24] S. Bieri, M. Serbyn, T. Senthil, and P. A. Lee, Phys. Rev. B **86**, 224409 (2012).
[25] L. Thompson and P. A. Lee, arXiv:1202.5655 (unpublished).
[26] P. Corboz, M. Lajkó, A. M. Läuchli, K. Penc, and F. Mila, Phys. Rev. X **2**, 041013 (2012).
[27] J. Nasu and S. Ishihara, arXiv:1209.0239 (unpublished).
[28] A. Mulder, R. Ganesh, L. Capriotti, and A. Paramekanti, Phys. Rev. B **81**, 214419 (2010).
[29] A. V. Chubukov, S. Sachdev, and T. Senthil, Nucl. Phys. B **426**, 601 (1994).
[30] C. Xu and S. Sachdev, Phys. Rev. B **79**, 064405 (2009).
[31] L. Capriotti, A. E. Trumper, and S. Sorella, Phys. Rev. Lett. **82**, 3899 (1999).
[32] A. F. Albuquerque, D. Schwandt, B. Hetényi, S. Capponi, M. Mambrini, and A. M. Läuchli, Phys. Rev. B **84**, 024406 (2011).
[33] Edited by Th. Hahn, *International Tables for Crystallography, Volume A: Space Group Symmetry* (Wiley, 2005, 5th edition).
[34] D. P. Arovas and A. Auerbach, Phys. Rev. B **38**, 316 (1988).
[35] N. Read and S. Sachdev, Phys. Rev. Lett. **66**, 1773 (1991).
[36] S. Sachdev, Phys. Rev. B **45**, 12377 (1992).
[37] T. Senthil and M. P. A. Fisher, Phys. Rev. B **62**, 7850 (2000).
[38] F. Wang and A. Vishwanath, Phys. Rev. B **74**, 174423 (2006).
[39] O. Tchernyshyov, R. Moessner and S. L. Sondhi, Europhys. Lett. **73**, 278 (2006).
[40] D. A. Huse, W. Krauth, R. Moessner, and S. L. Sondhi, Phys. Rev. Lett. **91**, 167004 (2003).
[41] M. Hermele, M. P. A. Fisher and L. Balents, Phys. Rev. B **69**, 064404 (2004).
[42] J. S. Bernier, Y.-J. Kao, and Y. B. Kim, Phys. Rev. B **71**, 184406 (2005).
[43] O. I. Motrunich, and T. Senthil, Phys. Rev. B **71**, 125102 (2005).
[44] B. I. Halperin, T. C. Lubensky, and S.-K. Ma, Phys. Rev. Lett. **32**, 292 (1974).
[45] M. J. Lawler, H.-Y. Kee, Y. B. Kim, and A. Vishwanath, Phys. Rev. Lett. **100**, 227201 (2008).
[46] C. H. Chung, J. B. Marston, and R. H. McKenzie, J. Phys. Condens. Matter **13**, 5159 (2001).
[47] M. Hammermesh, *Group Theory and Its Application to Physical Problems*, Dover Publications (1989).
[48] J. M. Luttinger and L. Tisza, Phys. Rev. **70**, 954 (1946).
[49] D. H. Lyons and T. A. Kaplan, Phys. Rev. **120**, 1580 (1960).
[50] D. Bergman, J. Alicea, E. Gull, S. Trebst and L. Balents, Nature Phys. **3**, 487 (2007).
[51] T.-P. Choy and Y. B. Kim, Phys. Rev. B **80**, 064404 (2009).
[52] J. P. Blaizot and G. Ripka, *Quantum Theory of Finite Systems* (MIT, Cambridge, MA, 1986).